CONFIGURATIONAL EVOLUTION DYNAMICS AND STABILITY DURING IN-SITU DEVELOPMENT OF LARGE ORBITING SPACECRAFT

AFOSR-91-0155

Final Technical Report

April 22, 1994

Anthony K. Amos
The Pennsylvania State University
Department of Aerospace Engineering
University Park, PA 16802

REPORT DOCUMENTATION PAGE

Form Approved
OMB No. 0704-0188

1. AGENCY USE ONLY (Leave blank)

2. REPORT DATE
22 April 1994

3. REPORT TYPE AND DATES COVERED
Final, Jan 15 1991 - 14 Jan 1994

4. TITLE AND SUBTITLE
Configurational Evolution Dynamics and Stability During In-Situ Development of Large Orbiting Spacecraft

5. FUNDING NUMBERS
AFOSR-91-0155

6. AUTHOR(S)
A K Amos

7. PERFORMING ORGANIZATION NAME(S) AND ADDRESS(ES)
The Pennsylvania State University
Dept of Aerospace Engineering
University Park, PA 16802

8. PERFORMING ORGANIZATION REPORT NUMBER
AFOSR-TR- 94 0361

9. SPONSORING/MONITORING AGENCY NAME(S) AND ADDRESS(ES)
AFOSR
110 Duncan Ave, Suite B115
Bolling AFB, DC 20332-0001

10. SPONSORING/MONITORING AGENCY REPORT NUMBER

11. SUPPLEMENTARY NOTES

12a. DISTRIBUTION/AVAILABILITY STATEMENT
Approved for Public Release; Distribution Unlimited

12b. DISTRIBUTION CODE

13. ABSTRACT (Maximum 200 words)

This report documents the objectives, major tasks and approaches of the research project, and the progress made over the three year span of the effort. The primary objective is presented as being the search for understanding of and analytical simulation capability for the effects of flexibility and configuration evolution on the on-orbit dynamics and stability of orbiting spacecraft. The approach is described in terms of the modeling and analysis of isolated deployment and assembly mechanisms, the modeling and analysis of coupled orbital-attitude-vibration dynamics of orbiting spacecraft, and the integration of the two for on-orbit system performance simulation. Details of the modeling and analysis efforts are described and sample results obtained during the scourse of the research are presented and discussed.

14. SUBJECT TERMS
Configuration Evolution, On-Orbit Dynamics, Stability of Spacecraft

15. NUMBER OF PAGES
48

16. PRICE CODE

17. SECURITY CLASSIFICATION OF REPORT	18. SECURITY CLASSIFICATION OF THIS PAGE	19. SECURITY CLASSIFICATION OF ABSTRACT	20. LIMITATION OF ABSTRACT
Unclassified	Unclassified	Unclassified	

TABLE OF CONTENTS

SUMMARY

This report documents the objectives, major tasks and approaches of the research project, and the progress made over the three year span of the effort. The primary objective is presented as being the search for understanding of and analytical simulation capability for the effects of flexibility and configuration evolution on the on-orbit dynamics and stability of orbiting spacecraft. The approach is described in terms of the modeling and analysis of isolated deployment and assembly mechanisms, the modeling and analysis of coupled orbital-attitude-vibration dynamics of orbiting spacecraft, and the integration of the two for on-orbit system performance simulation. Details of the modeling and analysis efforts are described and sample results obtained during the scourse of the research are presented and discussed.

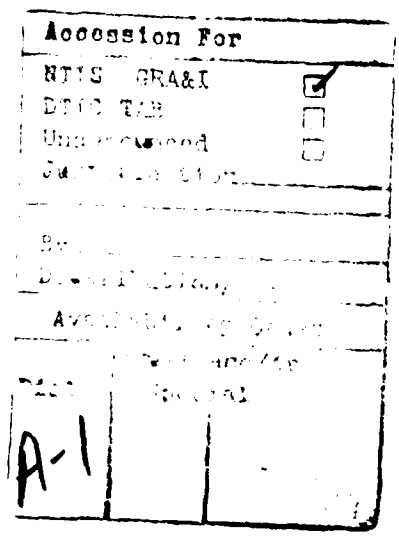

INTRODUCTION

This report describes progress made over the course of this research project. The primary objective was to investigate and delineate the effects of structural flexibility, deployment dynamics, and assembly mechanics on the dynamic performance, stability and controllability of flexible spacecraft systems. A secondary objective was to develop analytical tools for use in the simulation of the dynamics and control system performance of large space structures.

The motivation for the research is the need for improved base technologies to support future space missions in civilian and military applications. The national space program appears headed in the direction of a space station in low earth orbit to serve as a staging point and platform for vehicle construction and testing of large vehicles destined for lunar and martian human exploration and exploitation: the official goals of the US space program of the nineties and beyond. The construction of the space station will inevitably require on-orbit assembly of structural and other components transported from the earth, some of which might be of a deployable construction.

The military space objective is currently clouded by recent global political developments that have eliminated the soviet threat: the primary objective of military planning over the last couple of decades at least. Nevertheless, it is clear that the space segment of the basic military functions of communication, command and control will continue to expand in the future, and the military space assets will undoubtedly grow both in numbers and in sophistication. Servicing of these assets will require facilities for transportation among satellites, for refueling and repairing them in orbit, and for the berthing of these facilities in orbit. On-orbit construction of some of these assets will prove to be economically superior to the alternative of launching complete assemblies into orbit.

The technology pursued in this research can therefore be expected to have both military and civilian applications. The relevance of and need for the technology have been amply demonstrated in recent events such as the hang-up of the Galileo main antenna deployment mechanism, the recovery of the LDEF satellite from orbit which had to be accomplished extremely slowly in order to avoid suspected instabilities due to the flexibility of the RMS, the thermally induced vibrations in the solar panels of the Hubble Space Telescope that interfere with operations during transition from darkness to daylight, and the more recent difficulties with the deployment of the Italian tethered subsatellite in the summer of 1992.

RESEARCH TASKS

The research conducted under this project addressed itself to two major focus areas, as outlined below:

(a) Evolution Dynamics Characterization:

The goal here was to develop an understanding of basic deployment mechanisms, uncoupled from the spacecraft dynamics. Two deployment mechanisms were investigated: a two segment cantilevered telescoping mechanism illustrated in Figure 1, and a "planar Astromast" mechanism, illustrated in Figure 2.

The telescoping mechanism physical model consists of an inner and outer tube with the inner sliding freely relative to the outer. The outer tube is fixed. Figure 1 illustrates the model. The dynamic environment entails lateral vibrations in addition to the sliding (deployment) motion.

The "planar Astromast" model is illustrated in Figure 2. It is conceived to capture the deployment mechanism used in the actual Astromast design, within a simple model suitable for basic research. The Astromast design is a truss boom of triangular cross section, similar to the configuration shown in Figure 3. One end of the truss is held inside a cylindrical canister with helical grooved guides for the longerons of the truss. In its stowed configuration, the truss members are buckled and stacked inside the canister. Deployment is achieved by pushing the buckled members out of the canister continuously by a motorized geared system. As the members of each bay exit the canister, they snap into their straight configurations. Thus the deployment of the boom consists of continuous extrusion of truss bays, each accompanied by impulsive loads associated with the snapping into position of the buckled members.

This mechanism is duplicated in the planar truss model with respect to the buckling of truss members in the stowed configuration, the deployment by continuous extrusion out of a canister, and the snapping to shape of buckled members as each bay exits the canister. The conceptual design is a planar truss of lateral stays and diagonal members.

(b) Interaction with Orbital, Attitude and Structural Dynamics:

The telescopic deployment mechanism studied above was subsequently introduced into a generic orbiting spacecraft system, so that the effects of the configuration evolution on the orbital and attitude dynamics could be studied.

The generic spacecraft configuration is that of a dumbbell satellite with a telescoping flexible linkage between the two masses. It orbits the earth in a vertically oriented attitude: an inherently

stable configuration. The effects of deployment rate on the orbital and attitude motions were studied.

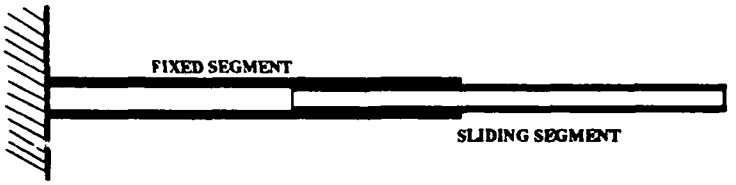

Figure 1. Telescopic Deployment Mechanism

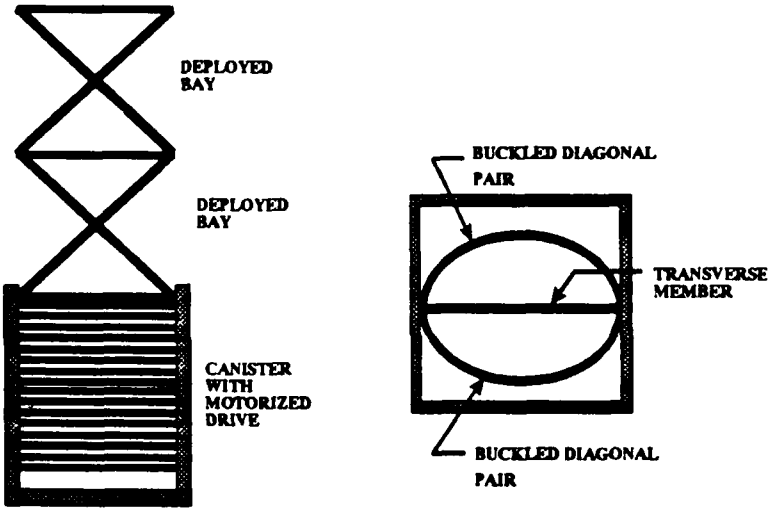

Figure 2. Planar "Astromast" Model

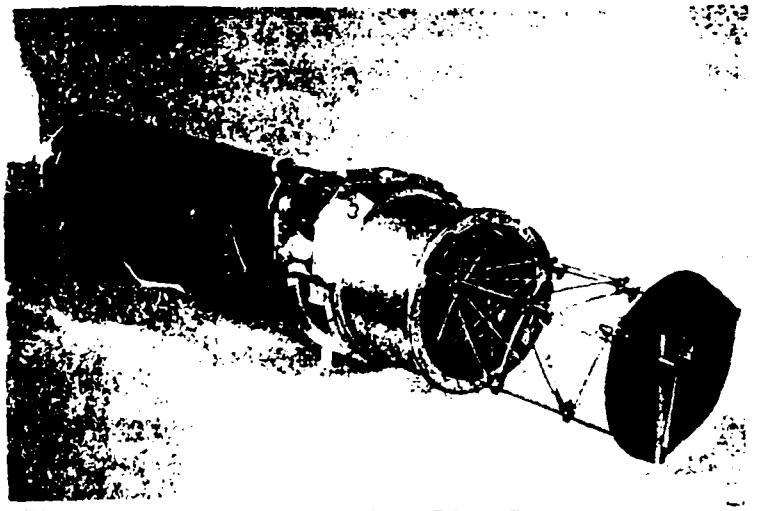

Figure 3. Model of the ASTROMAST Mechanism

ACCOMPLISHMENTS

(A) Isolated Deployment Mechanisms Modeling & Analyses

Telescoping Deployment

As previously reported the equations of motion have been derived based on the idealized model of Figure 4, and a linearized version of these basic dynamic equations has been used to study the variations of the modal characteristics with deployment stage. A phenomenon of modal agglomeration has been shown to arise for intermediate deployment stages primarily due to the discontinuities of mass and stiffness distributions associated with these stages. These results have been disseminated in one workshop presentation and an archival journal article.

The transient dynamics of the mechanism following an initial lateral deflection, with and without extrusion, have been studied using a combination of finite difference discretization in the spatial coordinates and numerical integration in the time coordinate by the Runge-Kutta fourth order scheme.

Equations of Motion

The equations of motion are a set of nonlinear non-autonomous partial differential equations (PDE's) derived in Appendix A of the *First Annual Technical Report* (*April 7, 1992*), and given by

$$m\ddot{u} - EA\frac{\partial^2 u_e}{\partial x^2} = 0 \tag{1}$$

$$m\left[\ddot{v} - \frac{1}{2}\left(\ddot{u}\frac{\partial v}{\partial x} + \dot{u}\frac{\partial \dot{v}}{\partial x} + \dot{v}\frac{\partial \dot{u}}{\partial x}\right)\right] + EI_y\frac{\partial^4 v}{\partial x^4} = P_y \tag{2}$$

$$m\left[\ddot{w} - \frac{1}{2}\left(\ddot{u}\frac{\partial w}{\partial x} + \dot{u}\frac{\partial \dot{w}}{\partial x} + \dot{w}\frac{\partial \dot{u}}{\partial x}\right)\right] + EI_z\frac{\partial^4 w}{\partial x^4} = P_z \tag{3}$$

where

m is the mass per unit length of each beam segment,
v and w are displacements in two orthogonal planes normal to the longitudinal axis of the beam,
u_e is the elastic longitudinal displacement,
EA, EI_y, EI_z are the axial and bending elastic rigidities of the beam, and
u is the resultant axial displacement reflecting deployment motion, elastic axial deformation, and fore-shortening of the beam axis with lateral displacements, and defined through its time derivative as shown below,

i.e., for the deploying segment

$$\dot{u} = U_D + \dot{u}_e - \frac{1}{2}\left(\dot{v}\frac{\partial v}{\partial x} + v\frac{\partial \dot{v}}{\partial x} + \dot{w}\frac{\partial w}{\partial x} + w\frac{\partial \dot{w}}{\partial x}\right) \tag{4}$$

and for the fixed segment

$$\dot{u} = \dot{u}_e - \frac{1}{2}\left(\dot{v}\frac{\partial v}{\partial x} + v\frac{\partial \dot{v}}{\partial x} + \dot{w}\frac{\partial w}{\partial x} + w\frac{\partial \dot{w}}{\partial x}\right) \tag{5}$$

where U_D is the deployment speed.

It is convenient to eliminate u from the first three equations using (4) or (5) and retaining only terms which are linear in the gradients $\partial u_e/\partial x$, $\partial v/\partial x$ and $\partial w/\partial x$ to yield for the deploying beam as an example

$$m\left[\ddot{u}_e + \dot{U}_D - \frac{1}{2}\frac{\partial^2}{\partial t^2}\left(v\frac{\partial v}{\partial x} + w\frac{\partial w}{\partial x}\right)\right] - EA\frac{\partial^2 u_e}{\partial x^2} \tag{6}$$

$$m\left[\ddot{v} - \frac{1}{2}\left(\ddot{u}_e\frac{\partial v}{\partial x} + \dot{u}_e\frac{\partial \dot{v}}{\partial x} + \dot{v}\frac{\partial}{\partial x}(\dot{u}_e)\right) - \frac{1}{2}\left(\dot{U}_D\frac{\partial v}{\partial x} + U_D\frac{\partial \dot{v}}{\partial x}\right)\right] + EI_y\frac{\partial^4 v}{\partial x^4} = p_y \tag{7}$$

$$m\left[\ddot{w} - \frac{1}{2}\left(\ddot{u}_e\frac{\partial w}{\partial x} + \dot{u}_e\frac{\partial \dot{w}}{\partial x} + \dot{w}\frac{\partial \dot{u}_e}{\partial x}\right) - \frac{1}{2}\left(\dot{U}_D\frac{\partial w}{\partial x} + U_D\frac{\partial \dot{w}}{\partial x}\right)\right] + EI_y\frac{\partial^4 w}{\partial x^4} = p_z \tag{8}$$

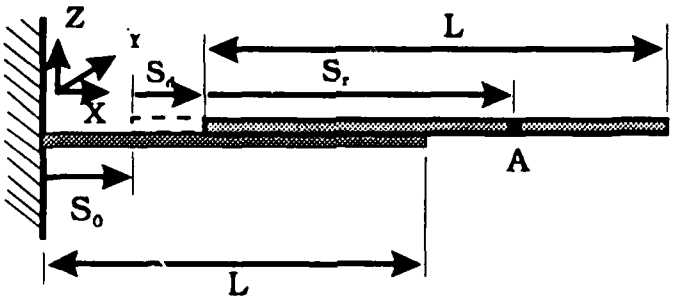

Figure 4. Idealized Model

Boundary and Interface Conditions

As shown in Figure 4, at the fixed end ($x = 0$), we have the boundary conditions

$$u_e = 0$$
$$v = v' = 0 \tag{9}$$
$$w = w' = 0$$

At the free end ($x = L + x_s$), we have

$$u'_e = 0$$
$$v'' = v''' = 0 \tag{10}$$
$$w'' = w''' = 0$$

At the ends of the overlap region, the cross sectional area and the bending rigidities of the compound beam change abruptly. However, the bending moments and the shear forces at these locations are, in the absence of external forces, continuous. Thus the second and third derivatives of the bending displacement functions are subject to the following jump conditions

$$\begin{aligned} EI_{y1}v''(x_s^-) &= EI_{y1}v''(x_s^+) & EI_{y1}v'''(x_s^-) &= EI_{y1}v'''(x_s^+) \\ EI_{z1}w''(x_s^-) &= EI_{z1}w''(x_s^+) & EI_{z1}w'''(x_s^-) &= EI_{z1}w'''(x_s^+) \\ EI_{y1}v''(L^-) &= EI_{y1}v''(L^+) & EI_{y1}v'''(L^-) &= EI_{y1}v'''(L^+) \\ EI_{z1}w''(L^-) &= EI_{z1}w''(L^+) & EI_{z1}w'''(L^-) &= EI_{z1}w'''(L^+) \end{aligned} \tag{11}$$

where x_s is shown in Figure 5 and the subscripts *1*, *2* and *3* refer to the correspondingly numbered zones in the same figure.

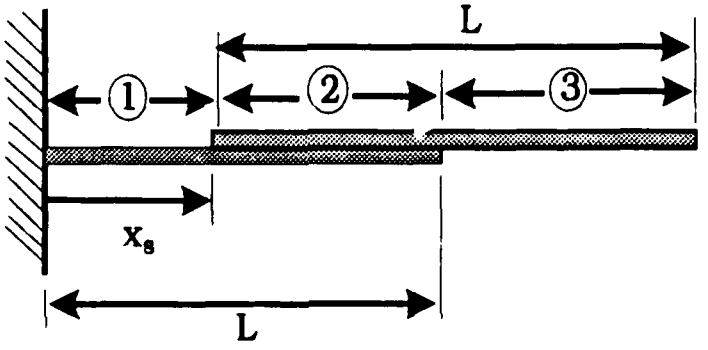

Figure 5. Zones of Uniform Properties

The displacement functions themselves and their first derivatives (bending slopes) are continuous at these locations, i.e.,

$$\begin{aligned} v(x_s^-) &= v(x_s^+) \qquad v'(x_s^-) = v'(x_s^+) \\ w(x_s^-) &= w(x_s^+) \qquad w'(x_s^-) = w'(x_s^+) \\ v(L^-) &= v(L^+) \qquad v'(L^-) = v'(L^+) \\ w(L^-) &= w(L^+) \qquad w'(L^-) = w'(L^+) \end{aligned} \tag{12}$$

Transient Response

Solutions of the governing equations (6), (7) and (8) are most expediently obtained by numerical integration, considering their nonlinear and non-autonomous nature. The solution algorithm developed consists of spatial discretization using second order central finite difference representations of the spatial derivatives, and implicit numerical integration of the resulting set of ordinary differential equations (ODE's) in time.

i) Finite Difference Discretization of Equations

The discretization process involves the application of the differential equations to a set of discrete points distributed more or less uniformly in the domain of the application. These computational grid points for the problem are illustrated in Figure 6 for the idealized telescopic beam.

The procedure is first described in its basic outline with respect to a single cantilevered uniform beam as illustrated in Figure 7, undergoing simultaneous axial and lateral vibrations with the latter confined to the x-y plane. Other features of the methodology necessary for adaptation to the problem on hand are described subsequently. For this simplified model the applicable equations are given by (6) and (7) subject to the appropriated boundary conditions from (9) and (10). The grid points are numbered 0 to n consecutively from left to right, the left point coinciding with the fixed end. Using equation (7) and applying it to the ith grid point yields

$$m\left[\ddot{v}_i - \frac{1}{2}\left(\ddot{u}_{ei}\overline{\frac{\partial v_i}{\partial x}} + \dot{u}_{ei}\overline{\frac{\partial \dot{v}_i}{\partial x}} + \dot{v}_i\overline{\frac{\partial \dot{u}_{ei}}{\partial x}}\right) - \frac{1}{2}\left(\dot{U}_D\overline{\frac{\partial v_i}{\partial x}} + U_D\overline{\frac{\partial \dot{v}_i}{\partial x}}\right)\right] + EI_y\overline{\frac{\partial^4 v_i}{\partial x^4}} = p_{yi} \tag{13}$$

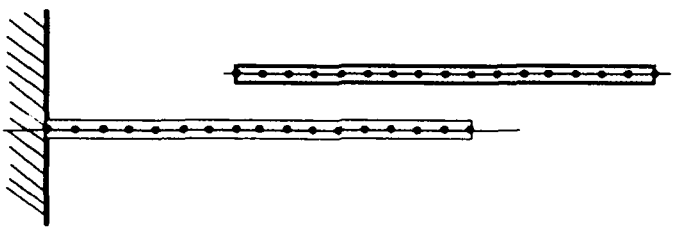

Figure 6. Computational Grid Points

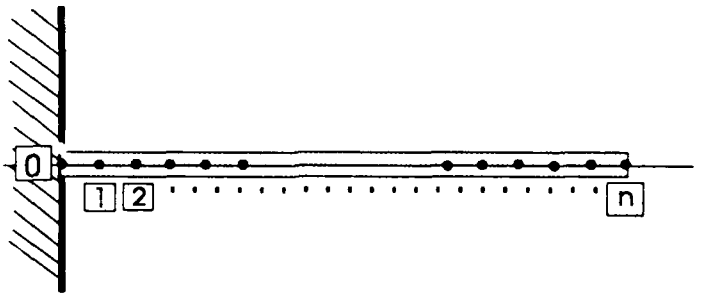

Figure 7. Isolated Beam Model

The spatial derivatives can now be replaced by their central finite difference equivalents

$$\frac{\partial v_i}{\partial x} = \frac{1}{2hL}(v_{i+1} - v_{i-1}) \qquad \frac{\partial \dot{v}_i}{\partial x} = \frac{1}{2hL}(\dot{v}_{i+1} - \dot{v}_{i-1})$$

$$\frac{\partial \dot{u}_{ei}}{\partial x} = \frac{1}{2hL}(\dot{u}_{e\,i+1} - \dot{u}_{e\,i-1}) \qquad \frac{\partial^4 v_i}{\partial x^4} = \frac{1}{h^4 L^4}(v_{i-2} - 4v_{i-1} + 6v_i - 4v_{i+1} + v_{i+2}) \tag{14}$$

where hL is the grid spacing. The result is the following ODE

$$\begin{aligned} m\ddot{v}_i - \frac{m}{4hL}\ddot{u}_{ei}(v_{i+1} - v_{i-1}) = p_{yi} &- \frac{EI_y}{h^4 L^4}[v_{i-2} - 4v_{i-1} + 6v_i - 4v_{i+1} + v_{i+2}] \\ &+ \frac{m}{4hL}\left[\dot{u}_{ei}(\dot{v}_{i+1} - \dot{v}_{i-1}) + \dot{v}_i(\dot{u}_{e\,i+1} - \dot{u}_{e\,i-1})\right] \\ &+ \frac{m}{4hL}\left[\dot{U}_D(v_{i+1} - v_{i-1}) + U_D(\dot{v}_{i+1} - \dot{v}_{i-1})\right] \end{aligned} \tag{15}$$

Considering the grid points (i = 1 ~ n) yields a set of n ODE's which can be expressed in matrix form as follows

$$\begin{aligned} m\begin{bmatrix} [0] & [I] & [0] \\ (nx2) & (nxn) & (nx2) \end{bmatrix}\{\ddot{v}\} + m\begin{bmatrix} [0] & [C(\{v\})] & [0] \\ (nx1) & (nxn) & (nx1) \end{bmatrix}\{\ddot{u}_e\} \\ = \frac{EI_y}{L^4}\{F_1(\mu_m, \{\sigma_p\}, \{v\}, \{\dot{v}\}, \{\dot{u}_e\}, U_D, \dot{U}_D)\} \end{aligned} \tag{16}$$

where

$$\{v\} = [v_{-1}, v_0, \ldots, v_n, v_{n+1}, v_{n+2}]^T$$

$$\{u_e\} = [u_{e0}, u_{e1}, \ldots, u_{en}, u_{e\,n+1}]^T$$

$$C_{ij} = \begin{cases} -\dfrac{1}{4h}(v_{i+1} - v_{i-1}) & j = i \\ 0 & j \neq i \end{cases}$$

$$F_{1i} = \sigma_{pi} - \frac{1}{h^4}[v_{i-2} - 4v_{i-1} + 6v_i - 4v_{i+1} + v_{i+2}] \tag{17}$$

$$+ \frac{\mu_m}{4h}\left[\dot{u}_{ei}(\dot{v}_{i+1} - \dot{v}_{i-1}) + \dot{v}_i(\dot{u}_{e\,i+1} - \dot{u}_{e\,i-1})\right]$$

$$+ \frac{\mu_m}{4h}\left[\dot{U}_D(v_{i+1} - v_{i-1}) + U_D(\dot{v}_{i+1} - \dot{v}_{i-1})\right]$$

$$\sigma_{pi} = \frac{p_{yi}L^4}{EI_y}; \qquad \mu_m = \frac{mL^3}{EI_y}$$

Defining

$$\{X_{R1}\} = [v_1, \ldots, v_n]^T \qquad \{X_{R2}\} = [u_{e1}, \ldots, u_{en}]^T \tag{18}$$

$$\{X_{E1}\} = [v_{-1}, v_{0,}, u_{e0}]^T \qquad \{X_{E2}\} = [v_{n+2}, v_{n+1}, u_{e\,n+1}]^T$$

equation (16) can be rewritten as

$$m[I]\{\ddot{X}_{R1}\} + m[C(\{v\})]\{\ddot{X}_{R2}\}$$

$$= \frac{EI_y}{L^4}\{F_1(\mu_m, \{\sigma_p\}, \{X_{R1}\}, \{\dot{X}_{R1}\}, \{X_{R2}\}, \{\dot{X}_{R2}\} \tag{19}$$

$$\{X_{E1}\}, \{\dot{X}_{E1}\}, \{X_{E2}\}, \{\dot{X}_{E2}\}, U_D, \dot{U}_D)\}$$

Note that for the simplified model of this analysis, the deployment speed U_D and acceleration $\dot{U}_D$ are identically zero. They have been retained in the equations for completeness of analytical treatment however.

Discretization and organization of equation (6) in an analogous manner yields a second set of equations as follows

$$m[D(\{v\})]\{\ddot{X}_{R1}\} + m[I]\{\ddot{X}_{R2}\} = \frac{EI_y}{L^4}\{F_2(\mu_m, \mu_a, \sigma_p, X_{R1}, \dot{X}_{R1}, X_{R2}, \dot{X}_{R2}, \{X_{E1}\}, \{\dot{X}_{E1}\}, \{X_{E2}\}, \{\dot{X}_{E2}\}, U_D, \dot{U}_D)\} \tag{20}$$

where

$$D_{ij} = \begin{cases} -\frac{1}{4h}(v_{i+1} - v_{i-1}) & j = i \\ -\frac{1}{4h}v_i & j = i+1 \\ \frac{1}{4h}v_i & j = i-1 \\ 0 & j < i-1,\ j > i+1 \end{cases} \tag{21}$$

$$F_{2i} = -\mu_m L\dot{U}_D + \frac{\mu_a}{h^2}(u_{e\,i+1} - 2u_{ei} + u_{e\,i-1}) + \frac{\mu_m}{2h}\dot{v}_i(\dot{v}_{i+1} - \dot{v}_{i-1}) \tag{22}$$

$$\mu_a = \frac{AL^2}{I_y}$$

Equations (19) and (20) can now be combined into

$$[A_R]\{\ddot{X}_R\} = \frac{EI_y}{mL^4}\{F(\{\sigma_p\}, \{X_R\}, \{\dot{X}_R\}, \{X_E\}, \{\dot{X}_E\}, U_D, \dot{U}_D, \mu_m, \mu_a)\} \tag{23}$$

where

$$\{X_R\} = \begin{Bmatrix} X_{R1} \\ X_{R2} \end{Bmatrix} \quad \{X_E\} = \begin{Bmatrix} X_{E1} \\ X_{E2} \end{Bmatrix} \quad [A_R] = \begin{bmatrix} I & C \\ D & I \end{bmatrix} \quad \{F\} = \begin{Bmatrix} F_1 \\ F_2 \end{Bmatrix} \tag{24}$$

ii) Discretization of Boundary Conditions

The first three in each of the boundary conditions (9) and (10) are applicable to the simplified model. Discretization of these by the central difference relations produces the set of algebraic equations

$$u_{e0} = 0$$

$$v_0 = 0$$

$$v'_0 = \frac{1}{2hL}(v_1 - v_{-1}) = 0$$

$$u'_{en} = \frac{1}{2hL}(u_{e\,n+1} - u_{e\,n-1}) = 0 \tag{25}$$

$$v''_n = \frac{1}{h^2L^2}(v_{n+1} - 2v_n + v_{n-1})$$

$$v'''_n = \frac{1}{2h^3L}(-v_{n+2} + 2v_{n-1} - 2v_{n+1} + v_{n-2}) = 0$$

from which the following relationship is easily established

$$\{X_E\} = \{G\}\,\{X_R\} \tag{26}$$

iii) Numerical Integration

Equation (26) can in principle be used to eliminate the extraneous variables $\{X_E\}$ from equation (23) resulting in the standard form

$$[A_R]\,\{\ddot{X}_R\} = \frac{EI_y}{mL^4}\{F(\{\sigma_p\}, \{X_R\}, \{\dot{X}_R\}, U_D, \dot{U}_D, \mu_m, \mu_a)\} \tag{27}$$

which is readily integrated by standard numerical integration schemes.

iv) Application to the Telescopic Beam

The procedure outlined above requires a number of enhancements in order to handle the unique features of the deploying telescopic beam, namely,

- deployment process,
- interaction between beam segments in the overlapping region.

The enhancements include

a. partitioning of the discretized equations for the separate segments between overlap and non-overlap grid points, and their combination to eliminate the unknown interaction forces, which are equal and opposite on the two segments;

b. provisions for satisfying the jump conditions of (11) through introduction of additional extraneous grid points;

c. relocation of grid points in the overlap region following each integration time step to account for the displacements caused by the deployment motion; and
d. derivation and use of non-standard finite difference representations for nonuniform grid spacing to accommodate the regridding scheme.

Relocation of grid points and use of non-standard finite difference representations are addressed in details here. During an integration time step, the grid points of the two beam segments in the overlap region which were coincident at the beginning undergo relative axial displacement due to deployment and results in grid point mismatches between the two segments. Further, the interior grid points at the ends of the overlap region are freed from contact with the other segment, thus transferring from the overlap region to the non-overlap zones. Our remedy is to relocate after each time step the grid points of the sliding segment in the overlap region for match up with those of the fixed segment and to introduce new interior grid points to correspond to the end points of the segments. While this restores coincidence of grid points between the two segments, it results in nonuniform spacing of the grid points near the ends of the overlap region. This necessitated the development of non-standard finite difference representations for irregular grid spacing. Figure 8 and Table 1 show the coefficients of the finite difference discretization of the fourth derivative $\partial^4 f/\partial x^4$ for both regular (standard approach) and irregular (non-standard) grid spacing.

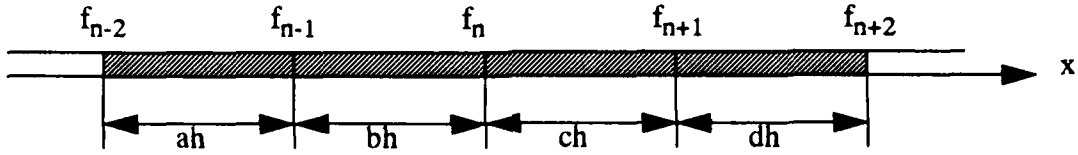

Figure 8. Second Order Finite Difference Discretization of $\frac{\partial^4 f_n}{\partial x^4}$

Table 1: Coefficients of Second Order Finite Difference Discretization of 4th Derivative

Coefficients	Regular Grid Points $a = b = c = d = 1$	Irregular Grid Points $a \neq b \neq c \neq d$ in general
c_{n-2}	1	$\frac{4!}{a(a+b)(a+b+c)(a+b+c+d)}$
c_{n-1}	-4	$\frac{-4!}{ab(b+c)(b+c+d)}$
c_n	6	$\frac{4!}{bc(a+b)(c+d)}$
c_{n-1}	-4	$\frac{-4!}{dc(b+c)(a+b+c)}$
c_{n-2}	1	$\frac{4!}{d(c+d)(b+c+d)(a+b+c+d)}$

Sample Results

i) Sample Problem

The beam segments are considered to be circular thin-walled tubes with the thickness to radius ratio sufficiently small to justify the approximation that the two segments have the same mass distribution and cross-sectional properties. The specific parameter groupings used in the sample analyses are:

ii) Transient Response to Initial deflections

Figure 9 shows the transient response and frequency spectra at selected locations of the beam at the 50% stage of deployment, following its release from an initially deflected state, in the absence of deployment motion. It is evident that the response is clearly a multi-mode one. All modes are observable near the root whereas only the first two dominate the tip response. The implication of this with respect to control sensor positioning is obvious.

Following the first two modes are several resonance-antiresonance frequency pairs, a classic phenomenon of interacting vibratory systems. The frequencies of these pairs start in the same range as the frequency coalescence phenomenon revealed by the eigenvalue analysis. The two observations are obviously related since both result from interaction of the two beam segments.

however, the exact nature of the relationship requires further study.

The transient response and frequency spectra at deployment stages of 25%, 45&, 65% and 85% are shown in Figures 10 through 13. They have the same features as the 50% deployment case.

Transient response in the presence of non-zero deployment velocity is depicted in Figure 14. It represents a snapshot at the 50% deployment stage of steady deployment at various constant speeds including zero speed. The time history and phase plane plots shown relate to the tip of the fixed segment. They clearly indicate that any deployment speed leads to an instability of the system. The degree of instability as manifested in the rate of amplitude growth with time increases with increasing deployment speed.

Any damping in the system, not considered in this analysis, will undoubtedly stabilize the system at the low deployment speeds but will become ineffective above some threshold speed above which the deploying system will again become unstable.

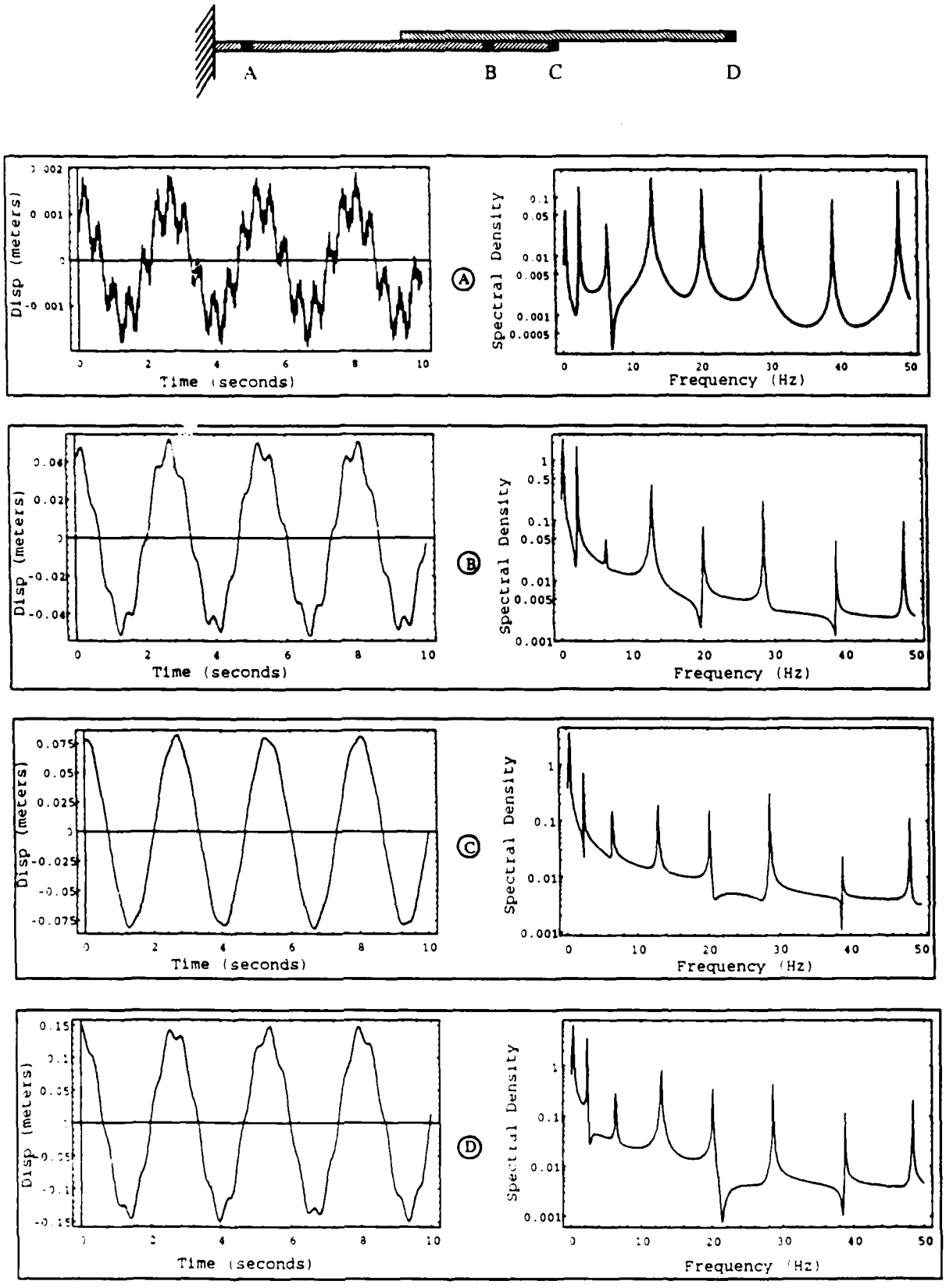

Figure 9. Transient Response at 50% Deployment: Zero Deployment Speed

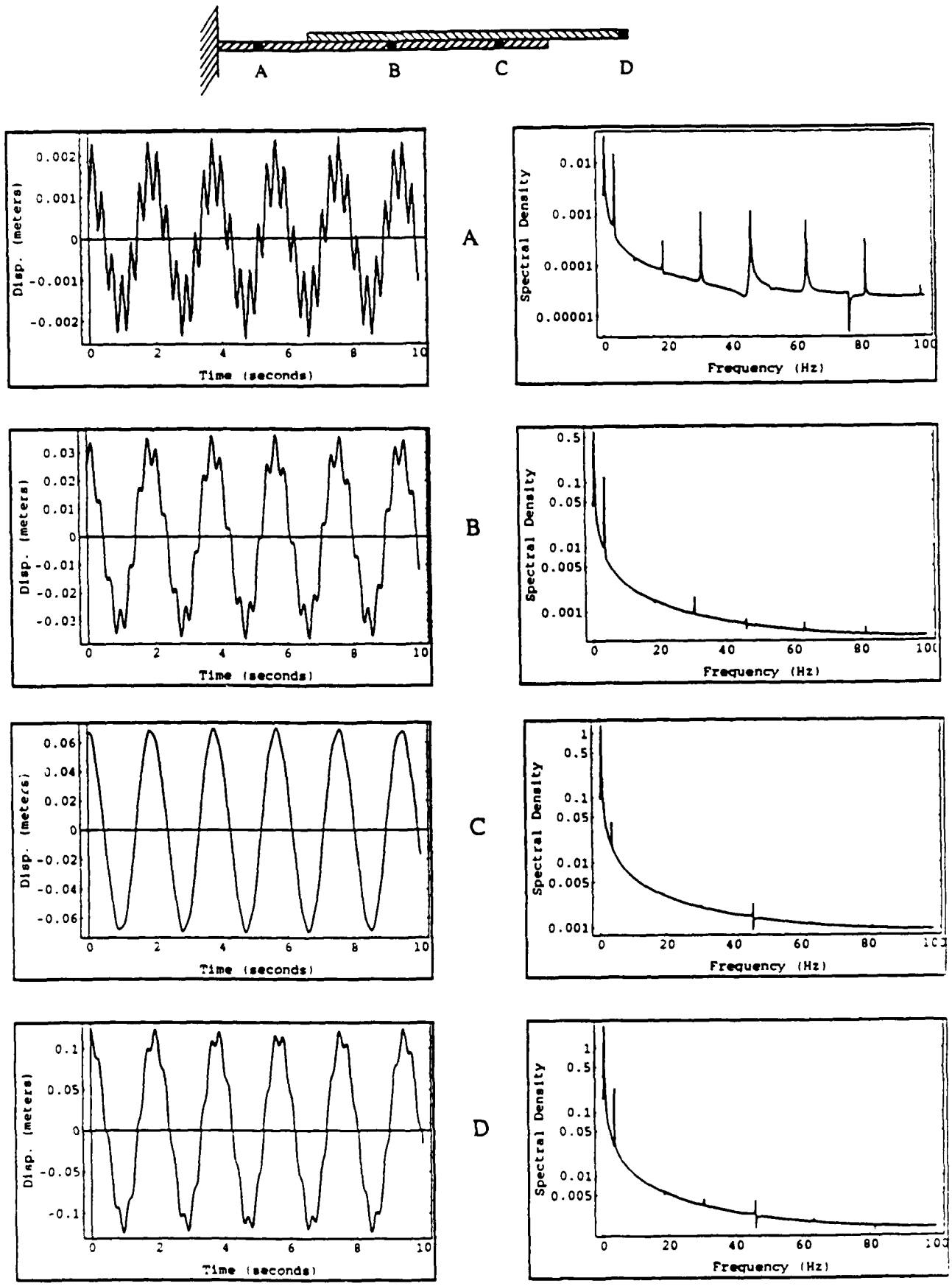

Figure 10. Transient Response at 25% Deployment: Zero Deployment Speed

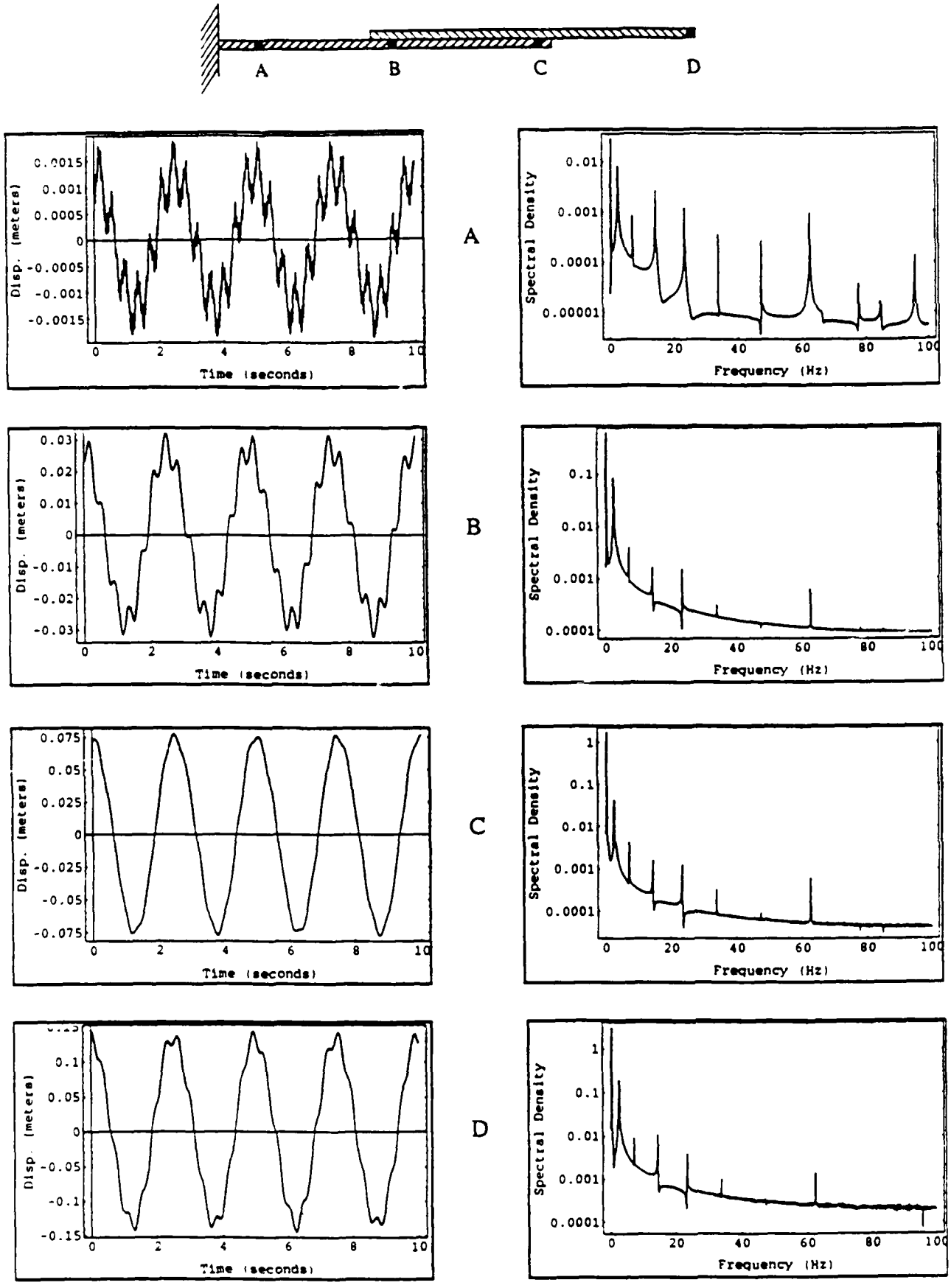

Figure 11. Transient Response at 45% Deployment: Zero Deployment Speed

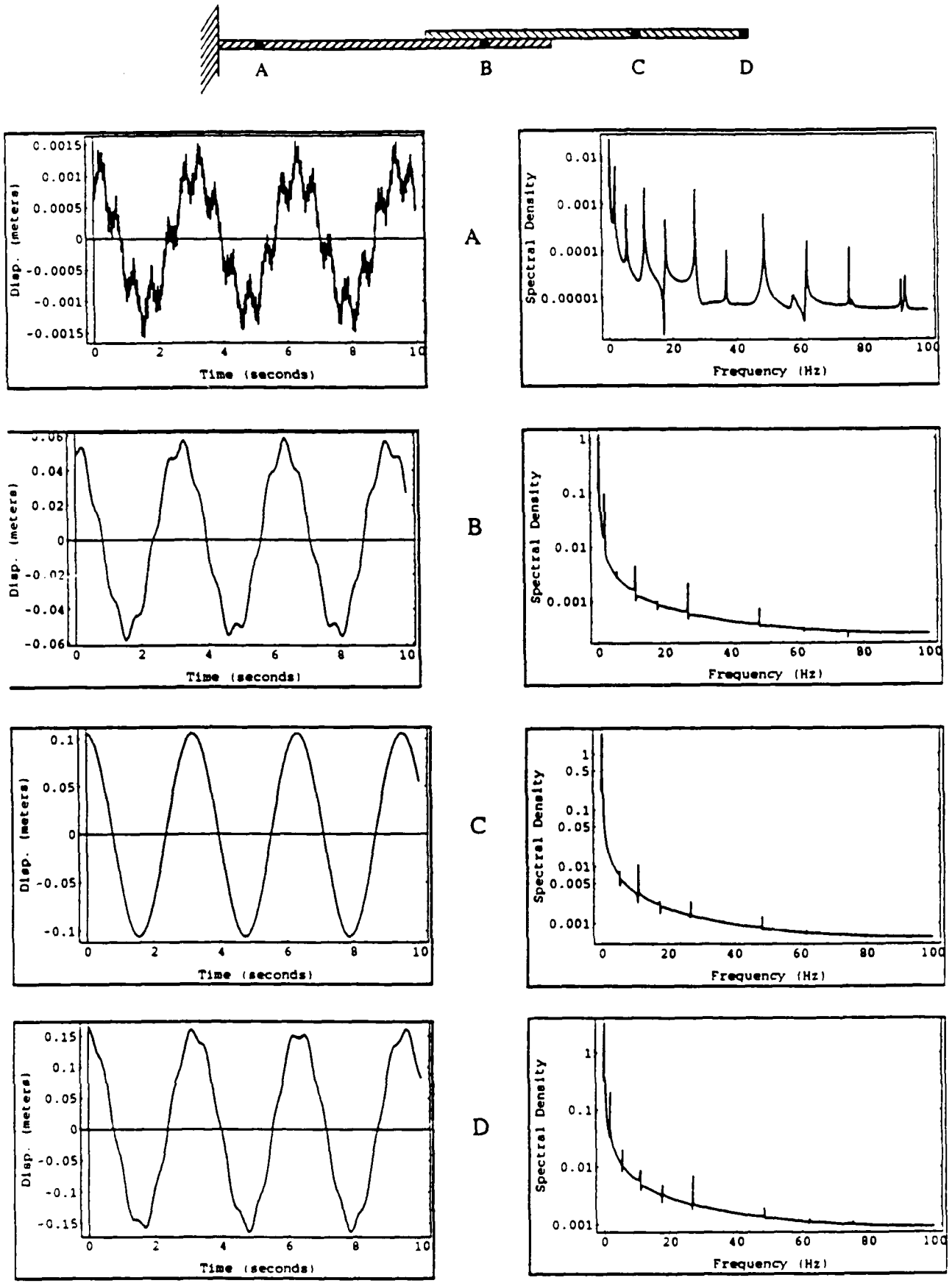

Figure 12. Transient Response at 65% Deployment: Zero Deployment Speed

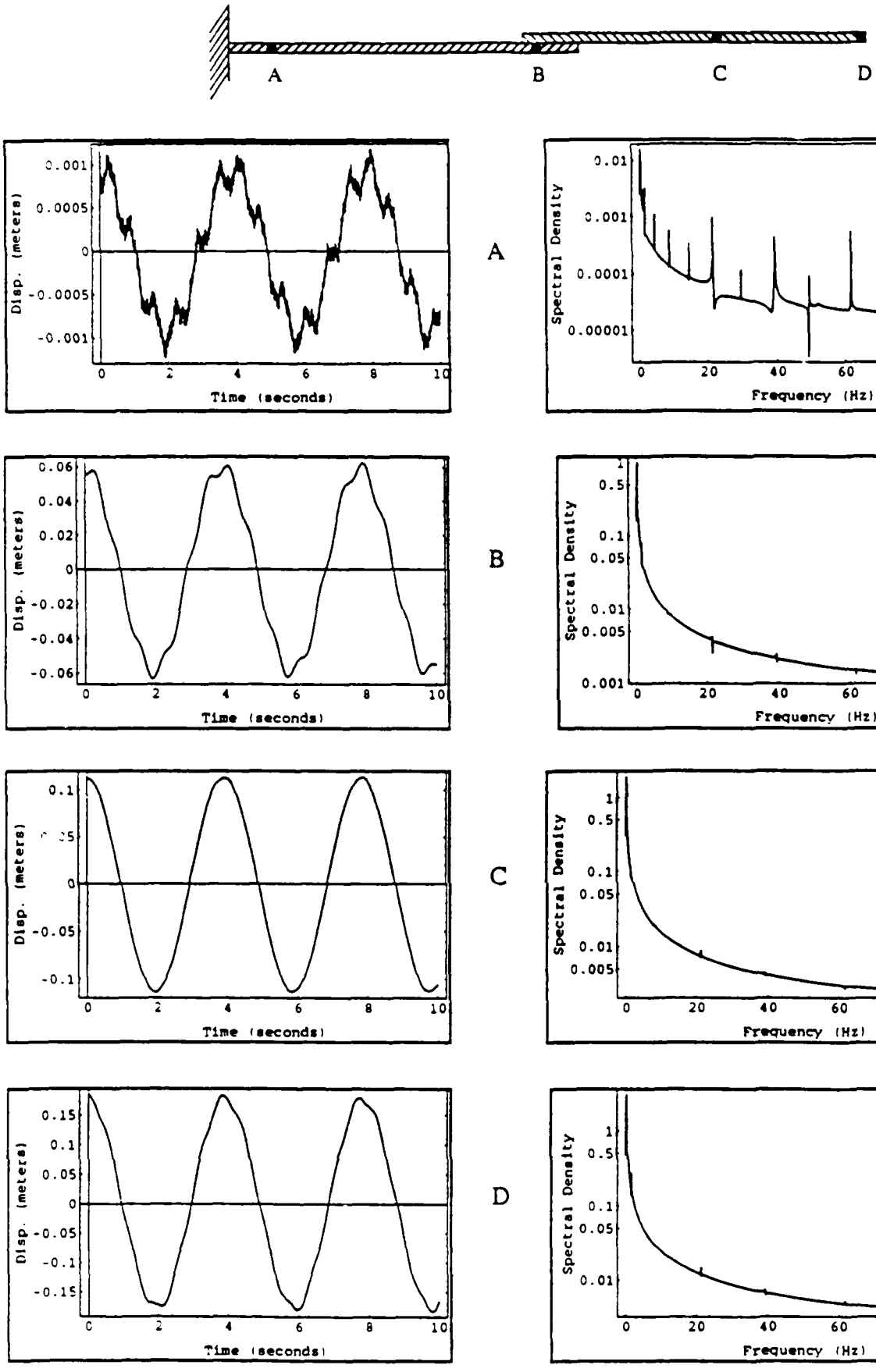

Figure 13. Transient Response at 85% Deployment: Zero Deployment Speed

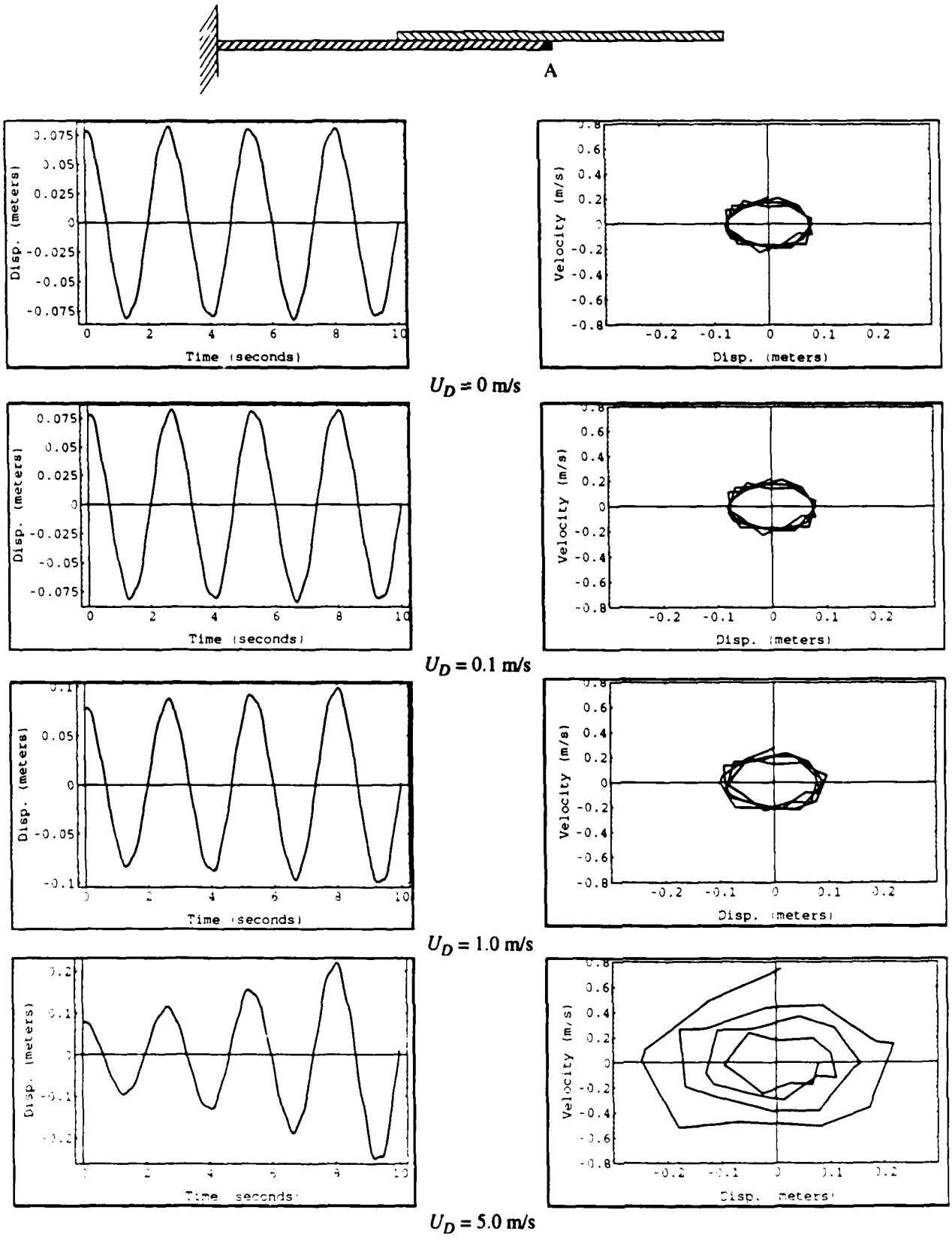

Figure 14. Transient Response at 50% Deployment: Various Deployment Speeds

Astromast Deployment

Efforts to date have concentrated on developing the dynamic equations of motion. Stability considerations require that the diagonal members be joined at their midpoints, which therefore make them behave as frame members rather than simple truss members. A hybrid truss-frame model has therefore been developed to aid in subsequent studies of this deployment mechanism. The modeling is conducted on a unit cell concept. A unit cell is a single bay of the extended configuration and consists of two diagonal members and a baton, as illustrated in Figure 15. The model of this unit cell serves as the building block for generating that of multi-bay configurations using modal synthesis techniques in the case of natural mode determination, and by means of interface compatibility constraint enforcement for transient analyses.

The variables of the unit cell model are the displacements of nodes 3, 4, and 5 in the x and y coordinate directions respectively (see Figure 15), and the corresponding nodal forces. The stiffness matrix relating the two is obtained from elementary beam theory as follows:

$$\{F\} = [K]\{\delta\} \tag{28}$$

where

$$\{F\} = [F_{3x}, F_{3y}, F_{4x}, F_{4y}, F_{5x}, F_{5y}]^T$$
$$\{\delta\} = [u_3, v_3, u_4, v_4, u_5, v_5]^T \tag{29}$$

$$K_{11} = 96k_1s^2 + 8k_2c^2 \qquad K_{26} = K_{62} = -(24k_1c^2 + 2k_2s^2)$$
$$K_{12} = K_{21} = 0 \qquad K_{33} = 12k_1s^2 + k_2c^2 + k_3$$
$$K_{13} = K_{31} = -24k_1s^2 - 2k_2c^2 \qquad K_{34} = K_{43} = (12k_1 - k_2)cs$$
$$K_{14} = K_{41} = -(24k_1 - 2k_2)cs \qquad K_{35} = K_{53} = -k_3$$
$$K_{15} = K_{51} = -(24k_1s^2 + 2k_2c^2) \qquad K_{36} = K_{63} = 0$$
$$K_{16} = K_{61} = (24k_1 - 2k_2) \qquad K_{44} = 12k_1c^2 + k_2s^2 \tag{30}$$
$$K_{22} = 96k_1c^2 + 8k_2s^2 \qquad K_{45} = K_{54} = K_{46} = K_{64} = 0$$
$$K_{23} = K_{32} = -(24k_1 - 2k_2)cs \qquad K_{55} = 12k_1s^2 + k_2c^2 + k_3$$
$$K_{24} = K_{42} = -(24k_1c^2 + 2k_2s^2) \qquad K_{56} = K_{65} = -(12k_1 - k_2)cs$$
$$K_{25} = K_{52} = (24k_1 - 2k_2)cs \qquad K_{66} = 12k_1c^2 + k_2s^2$$

$$k_1 = \left(\frac{EI}{L^3}\right)_{diagonal} \qquad k_2 = \left(\frac{EA}{L}\right)_{diagonal} \qquad k_3 = \left(\frac{EA}{L}\right)_{baton} \tag{31}$$

$$c = \cos\alpha \qquad s = \sin\alpha$$

The inertia matrix is generated by lumping the masses of the various members at the node points. The total mass of a member segment between adjacent nodes is divided equally between those nodes. For this investigation it is assumed that all members are from the same stock material and are identical in cross sectional properties. Specifically all members have the same mass per unit length m. The inertia matrix is thus a diagonal matrix with the following elements:

$$M_{11} = M_{22} = mL$$

$$M_{33} = M_{44} = M_{55} = M_{66} = \frac{mL}{4}(1 + 2\xi_B) \tag{32}$$

ξ_B = Length of baton/Length of diagonal

The unit cell modal characteristics are then obtained from the standard dynamic equation:

$$[M]\{\ddot{\delta}\} + [K]\{\delta\} = 0 \tag{33}$$

By non-dimensionalizing the inertia matrix with respect to mL, and the stiffness matrix by EI/L, the natural frequencies are obtained as

$$\omega_i = \beta_i \sqrt{\frac{EI}{mL^4}} \tag{34}$$

The frequency parameter β is then a function of the angle α and the ratio of axial and bending rigidities of the member stock.

For an illustrative sample calculation, the angle α is taken as 60° and the ratio of axial to bending rigidities as 3,000. The calculated frequency parameters and their corresponding mode shapes are shown in Table 2. Three of the modes (1,5,6) entail axial motion primarily while the other three (2, 3, 4) have appreciable lateral motions indicating them to be bending modes. The first axial mode is of particular interest since it has a very low frequency. As earlier indicated, the system would be a mechanism if the two diagonals were not pinned together. This constraint stabilizes some configurations of the mechanism, such as the first axial mode, but the bending rigidity of the diagonals is not sufficiently high to raise the frequency of the configuration into any measurable range.

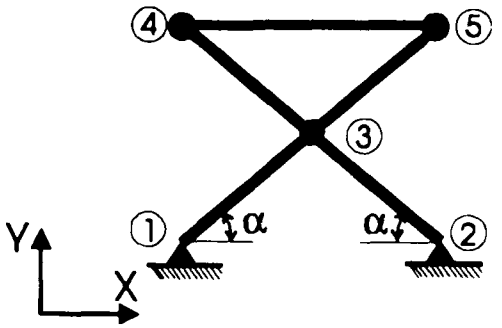

Figure 15. Unit Cell of Truss

Table 2: Parameters and Mode Shapes of Unit Cell

MODE #	β	MODE SHAPE
1	~0	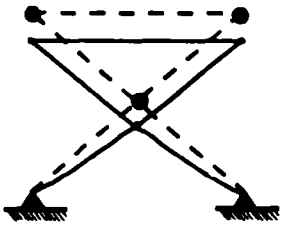
2	12.2	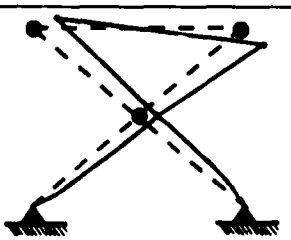
3	31.7	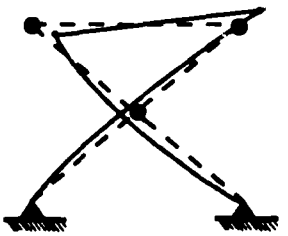
4	12.0E03	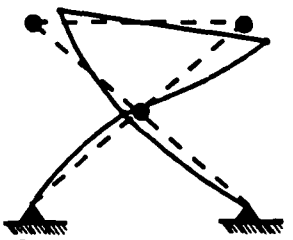
5	18.0E03	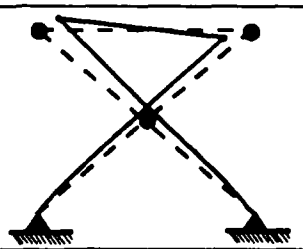
6	30.0E03	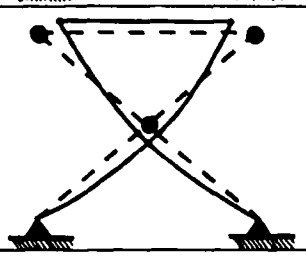

The modal characteristics of multi-bay deployed sections are obtained from the unit cell in two ways. One is a synthesis of the coefficient matrices of the multi-bay segment from those of the unit cell based on compatibility of displacements and deformations at the nodes where the different unit cells connect up. The second uses a component mode synthesis technique to generate the frequencies and mode shapes of the multi-bay segment from those of the unit cell. They yield identical results. Table 3 depicts the frequencies and mode shapes for the first five modes of a two-bay deployed segment. Here modes 1 2 and 4 represent the first, second and third bending modes respectively, whereas 3 and 5 represent axial modes.

The modal characterization capability developed here will enable dynamic simulations, including deployment, using modal coordinates. One such application in progress within a Master's thesis will investigate the dynamic response of multi-bay segments to the periodic impulsive excitation generated by the deployment process as buckled members unsnap during their extrusion from the canister. Since the excitation frequency is a function of the deployment speed, a resonance condition can be expected to arise at some critical deployment speed, leading to large amplitude oscillations. Furthermore, the flexibility of the deployed segment varies with the number of bays which increases continuously with the deployment process as a function of the deployment speed. Consequently, the resonance condition can be expected to exhibit a nonlinear relationship with the deployment speed, and jump and chaotic phenomena can be anticipated.

Table 3: Modal Parameters and Mode Shapes of 2-Bay Truss

Mode #	1	2	3	4	5
Frequency Parameter β	1.243	6.69	26.9	40.27	75.10
Mode Shape	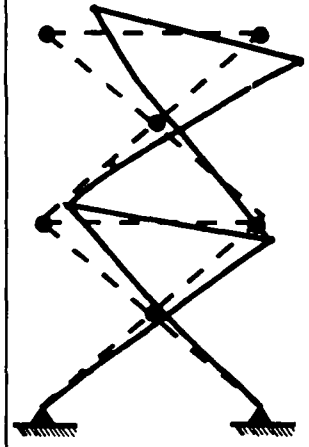	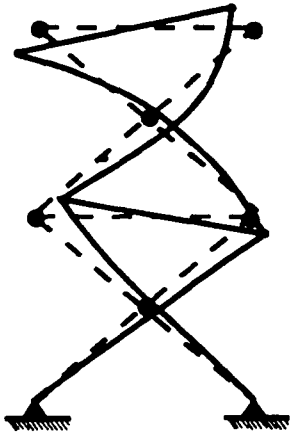	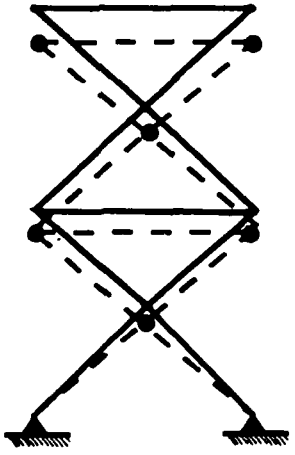	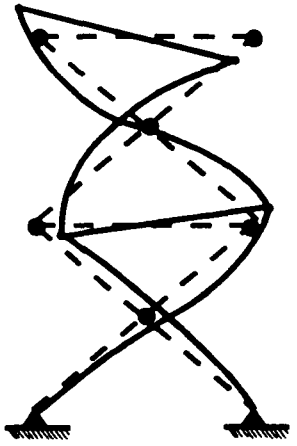	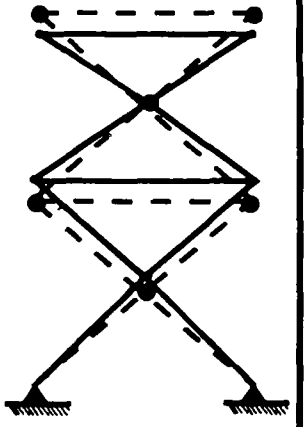

(B) Coupled Orbital-Attitude Dynamics Modeling & Analyses

In preparation for the study of the deployment mechanisms in orbit and also to permit analyses of docking maneuvers associated with assembly operations in space, a coupled orbital-attitude-and vibrational model has been developed and partially validated. Because of the complexity and highly nonlinear nature of the resulting equations, it has been necessary to conduct the validation at several levels of degeneration.

Planar Rigid Dumbbell Model:

By excluding the flexibility terms and restricting the rigid body motions to two-dimensional motions in the plane of the orbit, a planar rigid body model was obtained for the first level validation. This model is shown in Figure 16. The resulting equations are as follows:

$$[M_0]\begin{Bmatrix} \ddot{R} \\ \ddot{\theta} \\ \ddot{\psi} \end{Bmatrix} = \{F_0\} \tag{35}$$

where

$$[M_0] = \begin{bmatrix} m_T & -L_1\sin\psi & L_1\cos\psi \\ -L_1\sin\psi & (m_T R^2 + J_1 + 2RL_1\cos\psi) & -(J_1 + RL_1\cos\psi) \\ L_1\cos\psi & -(J_1 + RL_1\cos\psi) & J_1 \end{bmatrix} \tag{36}$$

$$\{F_0\} = \begin{bmatrix} L_1(\theta+\psi)\psi\cos\psi + m_T R\theta^2 + \theta(\theta+\psi)L_1\cos\psi + \dfrac{\mu}{R^2}\left(m_T - \dfrac{2L_1\cos\psi}{R}\right) \\ -2L_1 R\theta\cos\psi - 2R\dot{R}\theta + 2RL_1\theta\psi\sin\psi + RL_1\psi^2\sin\psi \\ -2L_1 R\theta\cos\psi - L_1\theta^2\sin\psi - \dfrac{\mu}{R^2}\left(L_1 - \dfrac{3J_1\cos\psi}{R}\right)\sin\psi \end{bmatrix} \tag{37}$$

with

$$m_T = m_1 + m_2 + m\ell; \quad L_1 = m_2 l + \frac{1}{2}ml^2; \quad J_1 = m_2 l^2 + \frac{1}{3}ml^3; \quad J_0 = J_1 + m_T R^2$$

While the problem of a rigid dumbbell in orbit has been considered by several investigators in the past, they have all been based on an assumption of a circular orbit. Therefore to validate the equations derived here, it was necessary to reduce the equations further to the case of a circular orbit by setting the time derivatives of the orbital radius and the orbital angular rate to zero. The resulting equations are in agreement with previous publications. They were used in a study [4] of the attitude librations of the dumbbell satellite as a function of the orbit eccentricity.

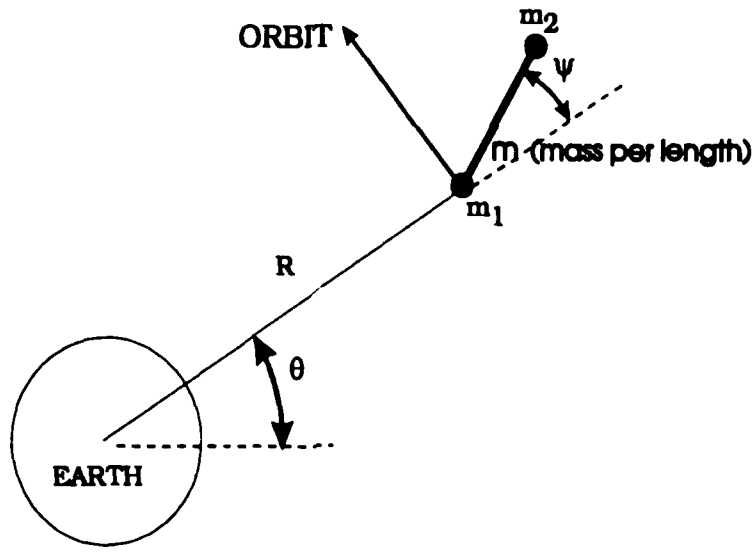

Figure 16: Planar Rigid Dumbbell Model

Planar Flexible Dumbbell Model:

A second level of degeneration retained the flexibility terms in a planar setting resulting in the planar flexible dumbbell model illustrated in Figure 17. The governing equations of motion are:

$$[M_0]\{\ddot{q}\} + \int_0^l [M_1]^T \ddot{w} ds = \{F_1\}$$

$$\left(\int_0^l [M_1] ds\right)\{\ddot{q}\} + \int_0^l m\ddot{w} ds = \int_0^l F_2 ds \tag{38}$$

where

$$[M_1] = m\left[\sin\psi \; -R\cos\psi \; -s\right]$$

$$\{F_1\} = \{F_0\} + \int_0^l m \begin{Bmatrix} -2(\dot{\theta}+\dot{\psi})\dot{w}\cos\psi \\ -2R(\dot{\theta}+\dot{\psi})\dot{w}\sin\psi \\ -2w\dot{w}\dot{\psi} \end{Bmatrix} ds \tag{39}$$

$$F_2 = m\left(\frac{-\mu}{R^2} + R\dot{\theta}^2\right)\sin\psi - EI\frac{\partial^4 w}{\partial s^4}$$

$$\{q\} = \left[R \; \theta \; \psi\right]^T$$

and $[M_0]$, $\{F_0\}$ are as defined for the rigid case.

These are a set of nonlinear integro-differential equations representing the orbital, attitude and flexibility dynamics of the dumbbell. The integral terms are mandated by the flexibility function w, which is a distributed parameter. For numerical solutions the flexibility contributions are discretized by means of a truncated basis function expansion. A Fourier odd series is the selected basis functions and is truncated at the third term for this application. i.e.

$$w(s,t) = \sum_{i=1}^{3} g_i(t) \sin\left(\frac{i\pi s}{l}\right) \tag{40}$$

Substituting this in equation (38), a set of governing ODE's are obtained as follows:

$$\begin{bmatrix} M_{11} & M_{12} \\ M_{12}^T & M_{22} \end{bmatrix} \begin{Bmatrix} \ddot{q} \\ \ddot{g} \end{Bmatrix} = \{F(q, \dot{q}, g, \dot{g})\} \tag{41}$$

where

$$[M_{11}] = \begin{bmatrix} m_T & -L_1\sin\psi & L_1\sin\psi \\ -L_1\sin\psi & (m_T K_1^2 + J_1 + 2L_1R_1\cos\psi) & -(J_1 + L_1R_1\cos\psi) \\ L_1\sin\psi & -(J_1 + L_1R_1\cos\psi) & J_1 \end{bmatrix}$$

$$[M_{12}] = \begin{bmatrix} \frac{2l}{\pi} & 0 & \frac{2l}{3\pi} \\ -\frac{2l}{\pi} & 0 & -\frac{2l}{3\pi} \\ \frac{l^2}{\pi} & -\frac{l^2}{2\pi} & \frac{l^2}{3\pi} \end{bmatrix} \qquad [M_{22}] = \frac{ml}{2}\begin{bmatrix} 1 & 0 & 0 \\ 0 & 1 & 0 \\ 0 & 0 & 1 \end{bmatrix} \qquad \{g\} = \begin{Bmatrix} g_1 \\ g_2 \\ g \end{Bmatrix} \tag{42}$$

$$F(1) = L_1(\dot{\theta}+\dot{\psi})^2\cos\psi + m_T\dot{\theta}^2 - \frac{\mu}{R^3}(m_T R - 2L_1\cos\psi) - \frac{4ml}{\pi}\left(\dot{g}_1 + \frac{\dot{g}_3}{3}\right)(\dot{\theta}+\dot{\psi})\cos\psi$$

$$F(2) = -2(m_T R - 2L_1\cos\psi)\dot{R}\dot{\theta} + L_1 R(2\dot{\theta}+\dot{\psi})\dot{\psi}\sin\psi - \frac{4ml}{\pi}R\left(\dot{g}_1 + \frac{\dot{g}_3}{3}\right)(\dot{\theta}+\dot{\psi})\sin\psi$$

$$F(3) = L_1(2\dot{R}\cos\psi + R\dot{\theta}\sin\psi)\dot{c} - \frac{\mu}{R^2}\left(L_1\sin\psi - \frac{3J_1}{R}\sin\psi\cos\psi\right) + ml(g_1\dot{g}_1 + g_2\dot{g}_2 + g_3\dot{g}_3)\dot{\psi}$$

$$F(4) = \frac{4ml}{\pi}\dot{R}\dot{\theta}\cos\psi + \frac{2ml}{\pi}R\dot{\theta}^2\sin\psi - \frac{2\mu ml}{\pi R^2}\sin\psi + \frac{ml}{2}(\dot{\theta}+\dot{\psi})^2 g_1 - \frac{EIl}{2}\left(\frac{\pi}{l}\right)^4 g_1$$

$$F(5) = \frac{ml}{2}(\dot{\theta}+\dot{\psi})^2 g_2 - \frac{EIl}{2}\left(\frac{2\pi}{l}\right)^4 g_2$$

$$F(4) = \frac{4ml}{3\pi}\dot{R}\dot{\theta}\cos\psi + \frac{2ml}{3\pi}R\dot{\theta}^2\sin\psi - \frac{2\mu ml}{3\pi R^2}\sin\psi + \frac{ml}{2}(\dot{\theta}+\dot{\psi})^2 g_3 - \frac{EIl}{2}\left(\frac{\pi}{l}\right)^4 g_3$$

These equations are strongly coupled, highly nonlinear, and very stiff. The stiffness arises from the fact that the orbital and attitude parameters of R, θ and the flexibility parameters of g have typical values that are several orders of magnitude different, and contain frequencies that are an order of magnitude or two apart. To avoid possible numerical difficulties in the integration of the equations, the latter are preconditioned by a standard perturbation analysis which separates the orbital and attitude parameters into nominal and perturbation components, with the perturbation components being of the same order of magnitude as the flexibility parameters. The governing equations are in the process segregated into a nominal set and a perturbation set which are integrated sequentially. Details of this preconditioning procedure are given in [3].

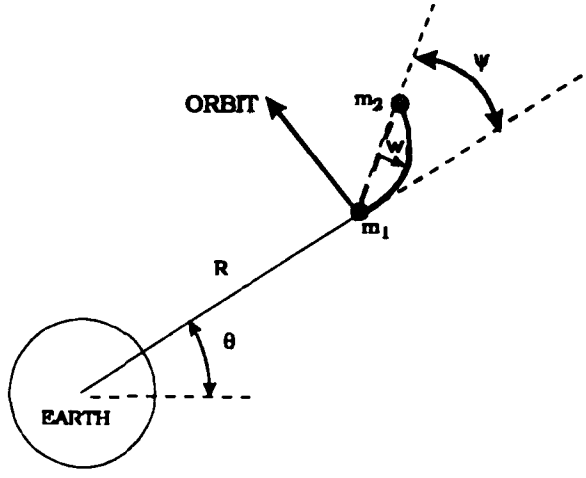

Figure 17: Planar Flexible Dumbbell Model

On-orbit Maneuvers - Planar Flexible Dumbbell:

The equations developed above were used in [3] to simulate the dynamics of a flexible dumbbell undergoing two routine orbital maneuvers: orbit circularization from an elliptical orbit, and a Hohmann transfer. Almost all spacecraft launched from the earth obtain orbit insertion on an elliptical orbits, and must undergo the circularization maneuver if the final orbit is required to be circular. This is typically performed at apogee (highest altitude of elliptical orbit) by firing

"apogee motors" to increase the spacecraft velocity to that required for a circular orbit at the apogee altitude. If the desired circular orbit altitude is less than that at apogee then the maneuver must be performed outside apogee. Our study examines both scenarios for this maneuver. The second maneuver is used for fuel efficient transfer between two circular orbits of different altitudes. It involves two firings of the orbital transfer thrusters: once to transition from the initial circular orbit to an elliptical transfer orbit, and the second time to transition from the transfer orbit to the final circular orbit. The transfer orbit will thus have its perigee and apogee at the two transition points.

Each simulation is initiated by specifying initial values of the orbital radius and azimuth and their corresponding rates, the attitude angle and rate, and the flexibility variables and rates. The initial orbital parameters are pre-calculated to drive the simulation to the desired initial orbit. The attitude paraters are specitfied to correspond to the nominal attitude, which for these studies was taken as the vertical or radial configuration. The flexibility effects were always started from rest. The differential equations of motion are integrated forward in time till the orbit is well established and the transition conditions have been achieved. The time rates of the orbital and attitude parameters are then changed by amounts corresponding to pre-computed impulsive velocity changes resulting from the firing of the maneuvering thrusters.

Figure 18 illustrates the orbit circularization maneuver. The more common form with transition occurring at apogee is on the left, and the off-apogee maneuver is on the right. The resulting dynamics for the case of circularization at apogee are shown in Figure 19. The maneuver in this case takes place after 40,000 seconds or seven and a half orbits into the flight. The top figure represents the time history of the attitude angle. Immediately below are two phase plane plots representing the motions before and after the transition.They show that the attitude motion for the initial elliptical orbit is quasi-periodic with an amplitude of about 0.02 radians, and changes to a much lower amplitude periodic motion after circularization.The vibrations of the flexible linkage are represented by the time history and phase plane plots shown on the third and fourth rows. Again we observe a transition from quasi-periodic oscillation before the maneuver to an almost periodic vibrations afterwards. The amplitude of the periodic vibrations is slightly reduced from the peaks of the quasi-periodic vibrations. The last row shows the spectral density of the linkage vibrations before and after circularization. The quasi-periodicity is due to the presence of three dominant frequencies corresponding to the orbital, attitude and vibrational frequencies. The periodic vibration is dominated by the vibrational frequency with a slight corruption by the attitude frequency.

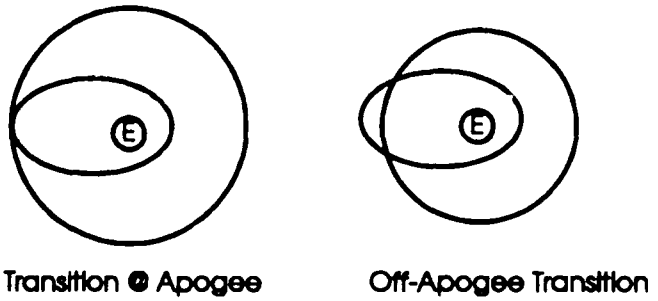

Figure 18: Orbit Circularization Maneuvers

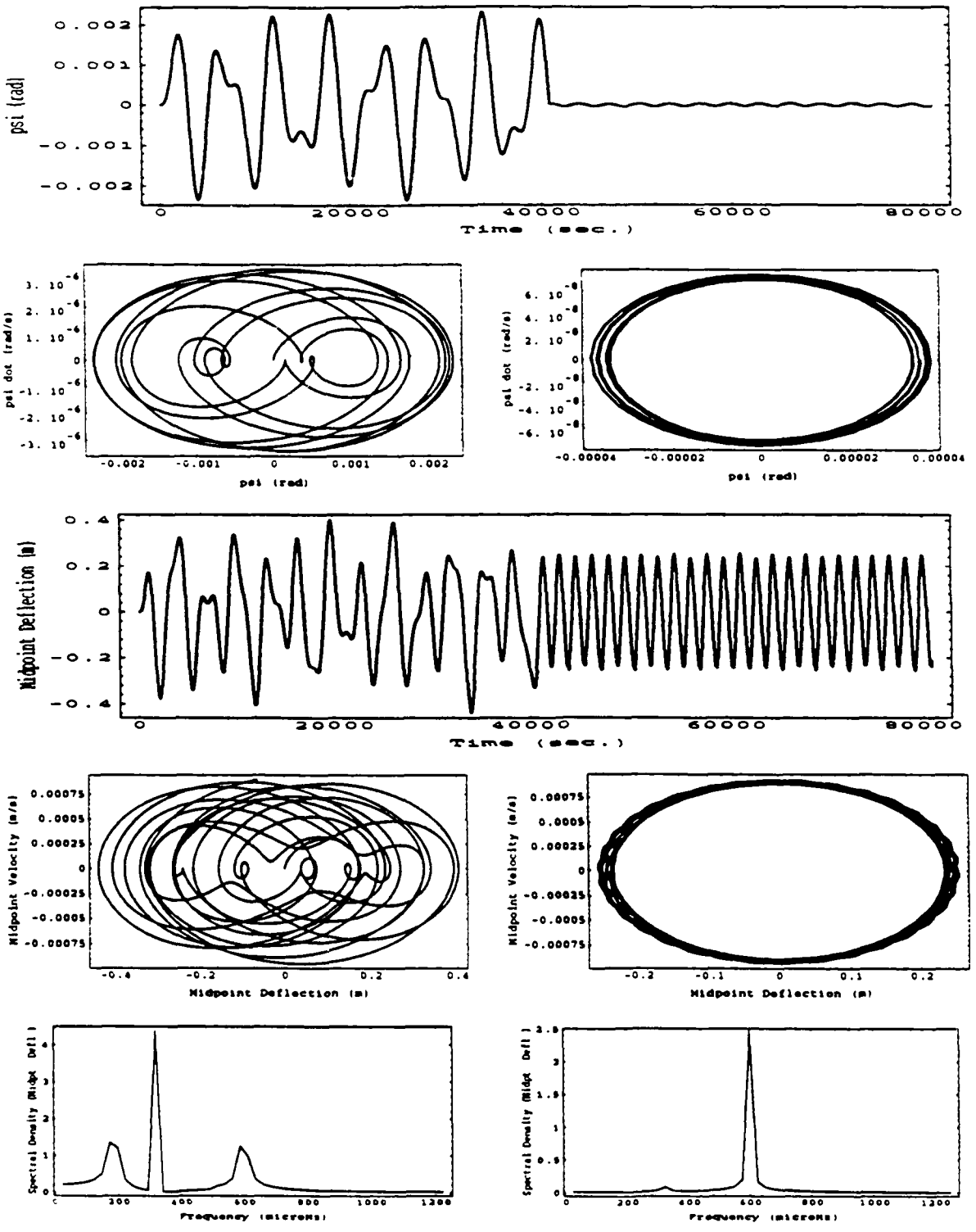

Figure 19: Attitude and Vibrational Dynamics for Orbit Circularization Maneuver Initiated at Apogee

Figure 20 presents the results of the off-apogee maneuver simulation. The time histories at the top represent the librational and linkage vibrational motions respectively. Below them are phase plane and spectral density plots of the two motions after circularization. In contrast with the apogee variety, the attitude motion after circularization continues at about the same amplitude as before the maneuver, and is quasi-periodic, with the orbital frequency continuing to exert significant influence even after circularization. The linkage vibration shows appreciable amplification after the maneuver and is also quasi-periodic. The vibration at its own natural frequency is overshadowed by that at the attitude frquency.

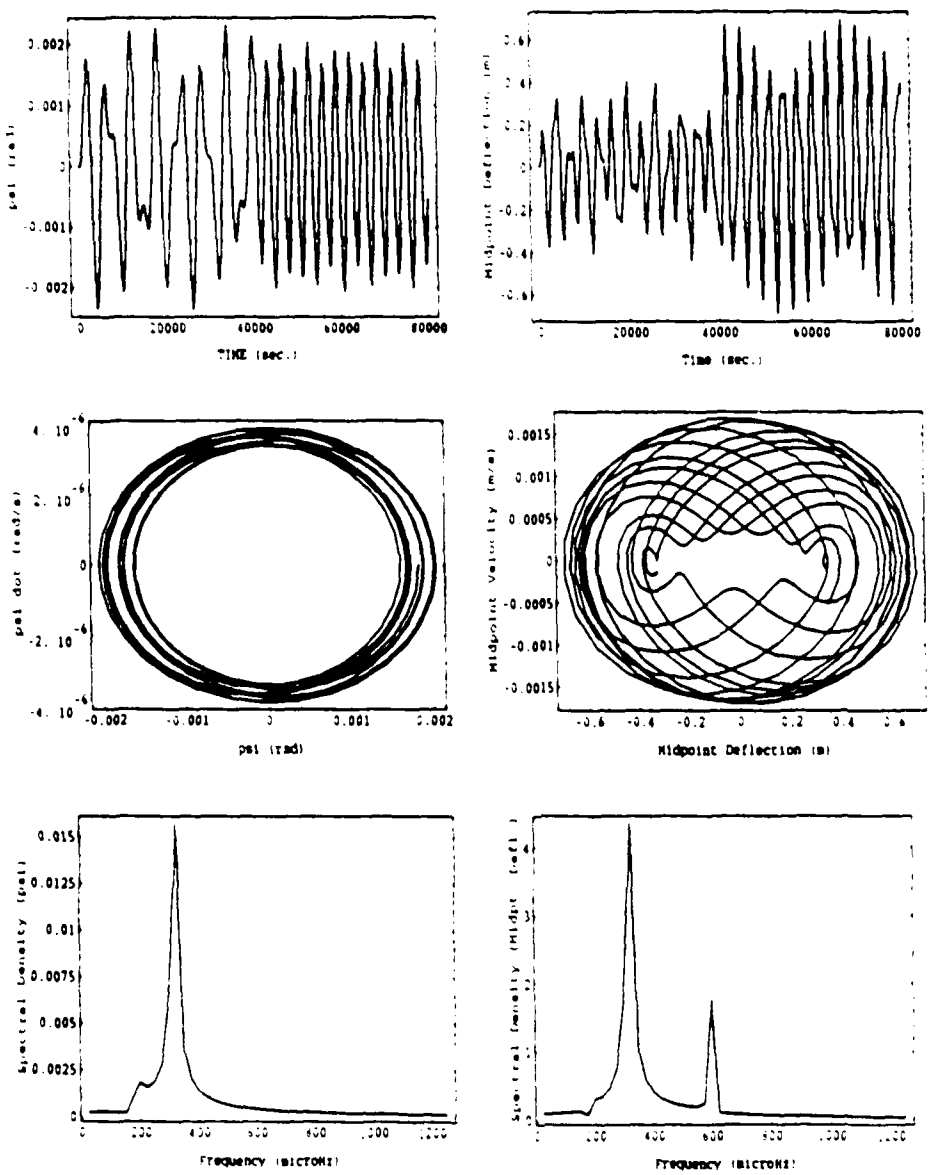

Figure 20: Attitude and Vibrational Dynamics for Orbit Circularization Maneuver Initiated Off-Apogee

The Hohmann transfer maneuver is illustrated schematically in Figure 21, and simulation results are shown in Figure 22. The spacecraft transfers from a circular orbit of 6,700 kilometer altitude to a geosynchronous altitude. The attitude time history is shown at the top. It is characterized by the absence of any perceptible librations throughout the initial circular orbit of about 6,000 seconds duration (one orbit). The first impulse to transition to the elliptical transfer orbit sets the dumbbell tumbling end-on-end until it is arrested by the second impulse after rotating through 5π radians. It then remains in the upside-down attitude as it transitions to the second circular orbit. The linkage vibration motion is shown in various formats in the remaining plots. The first is a time history plot, and is followed by a phase-plane and spectral density pair for the initial circular orbit phase. The next two rows show the corresponding plots for the transfer orbit and final circular orbit phases respectively. They provide the following picture of the vibrational behavior during the maneuver:

- The vibration during the initial circular orbit phase is extremely small. It is however quasi-periodic at its own frequency and the attitude frequency.
- The first pulse produces a large transient excursion which quickly settles down to a small amplitude oscillations.
- These are initially quasi-periodic with significant responses at the attitude and dominant modal frequencies.
- The amplitude remains pretty constant during the second impulse, and the motion becomes periodic over the last circular orbit.

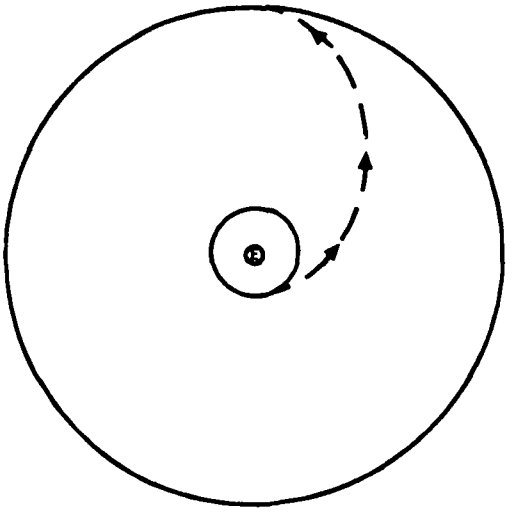

Figure 21: The Hohmann Transfer Maneuver

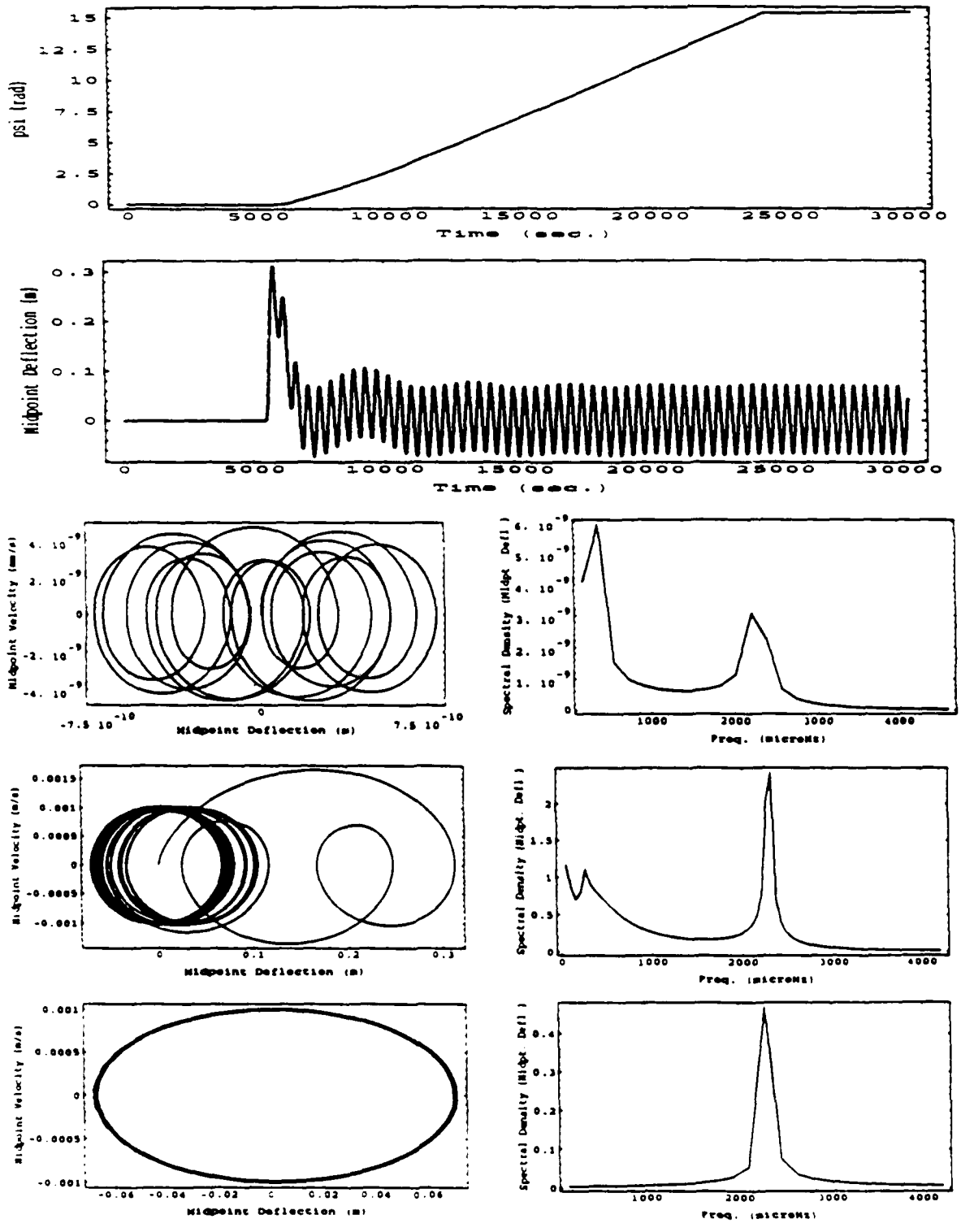

Figure 22: Attitude and Vibrational Dynamics for Hohmann Transfer Maneuver

(C) Coupled Orbital-Attitude-Vibration-Deployment Dynamics

We now consider the flexible dumbbell to be deployable by incorporating a flexible telescopic beam as the linkage between the two masses. We limit our consideration to a two segment mechanism, and we explore the dynamics of this spacecraft in orbit, undergoing both librational motions in the plane of the orbit simultaneously with deployment and attendant vibrations, also assumed to be confined to the orbital plane. A model of this system is illustrated in Figure 23.

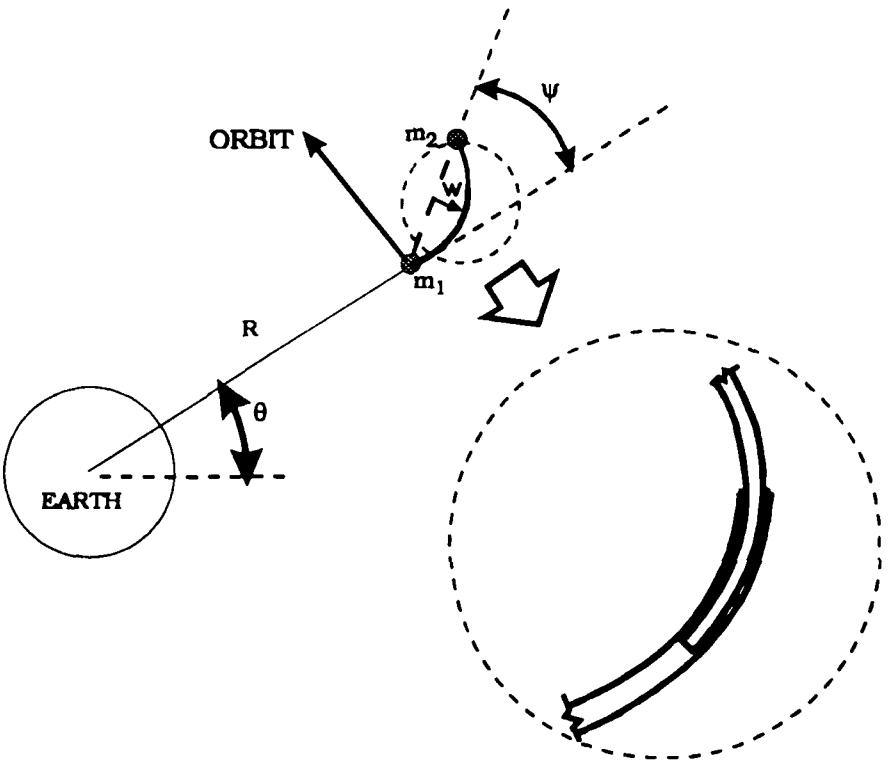

Figure 23:Planar Deployable Flexible Dumbbell Model

The orbital, attitude and vibrational motions are governed by the equations derived for the satellite without the deployment mechanism (equations 38) together with additional terms arising from the axial degree of freedom introduced by the mechanism and its dynamic couplings with the other degrees of freedom. i.e.

$$\left[M_0 + M_o^u\right]\{\ddot{q}\} + \int_0^{\ell}\left[M_1 + M_1^u\right]^T \ddot{w}\,ds + \int_0^{l} M_2^u \ddot{u}\,ds = \{F_1 + F_1^u\}$$

$$\left(\int_0^{\ell}\left[M_1 + M_1^u\right]ds\right)\{\ddot{q}\} + \int_0^{\ell} m\ddot{w}\,ds = \int_0^{\ell}(F_2 + F_2^u)\,ds \qquad (43)$$

An additional equation of the form shown below governs the deployment process.

$$\int_0^l \left(\left[M_2^u \right] \{\ddot{q}\} + M_3^u \ddot{w} + m\ddot{u} \right) ds = \int_0^l F_3^u ds \tag{44}$$

For the studies reported herein these equations were further simplified by ignoring the flexibility effects in order to explore the consequences of the deployment dynamics interactions with the orbital and attitude dynamics. Thus the results apply to a rigid dumbbell satellite with a telescopic deployment mechanism.

Initial simulations were performed primarily to verify the new code. By setting the deployment speed to zero, simulation results could be compared directly with previous results for the non-deploying satellite. Additional simulations were also conducted to study the effects of variations in the distance between the two masses as a result of the deployment.

Figure 24 shows the simulation results for a a fully stowed dumbbell in a vertical attitude initially. It is set in motion with an orbital angular velocity corresponding to that of an isolated mass at the mass 1 location in a circular orbit. On the left are the time history, phase-plane and spectral density plots of the orbital motion. On the right are similar plots for the attitude angle. It is easily observed that the orbit of the reference mass (mass 1) is slightly eccentric with the radius varying between the periapsis and apoapsis values of 19.200×10^3 and 19.203×10^3 kilometers. The corresponding eccentricity is 0.73×10^{-4}. The orbital motion is essentially circular. The orbital frequency of approximately 4.00×10^{-4} hertz is also evident from the spectral density plot. The attitude motion (libration) is a quasi-periodic oscillation about the initial vertical attitude, and is dominated by two components at the orbital frequency and the attitude frequency of 6.50×10^{-4} hertz approximately. The maximum amplitude of the librational motion is about 1.0×10^{-4} radians. Calculations of total mechanical energy and angular momentum about the focus yielded values that remained constant over the length of the simulation. These results indicate that the initial vertical attitude is stable in orbit

Similar results were obtained for the dumbbell in a 25% and 75% deployed configurations. These are shown in Figures 25 and 26. The effects of the increasing inter-mass separation are slight increases in orbital eccentricity and libration amplitude. These results are in total agreement with previous data for the rigid dumbbell without the deployment mechanism.

In the next series of simulations, the dumbbell was allowed to deploy from the fully collapsed to the fully deployed configuration at a constant speed of 0.0025 meters per second. In the first case the initial attitude was set as the local vertical, just as in the previous simulations. The results are shown in Figure 27. Again the orbital motion charts are on the left and the attitude ones are on the right. The orbit time history and phase-plane plot show a transient phase lasting about three orbits

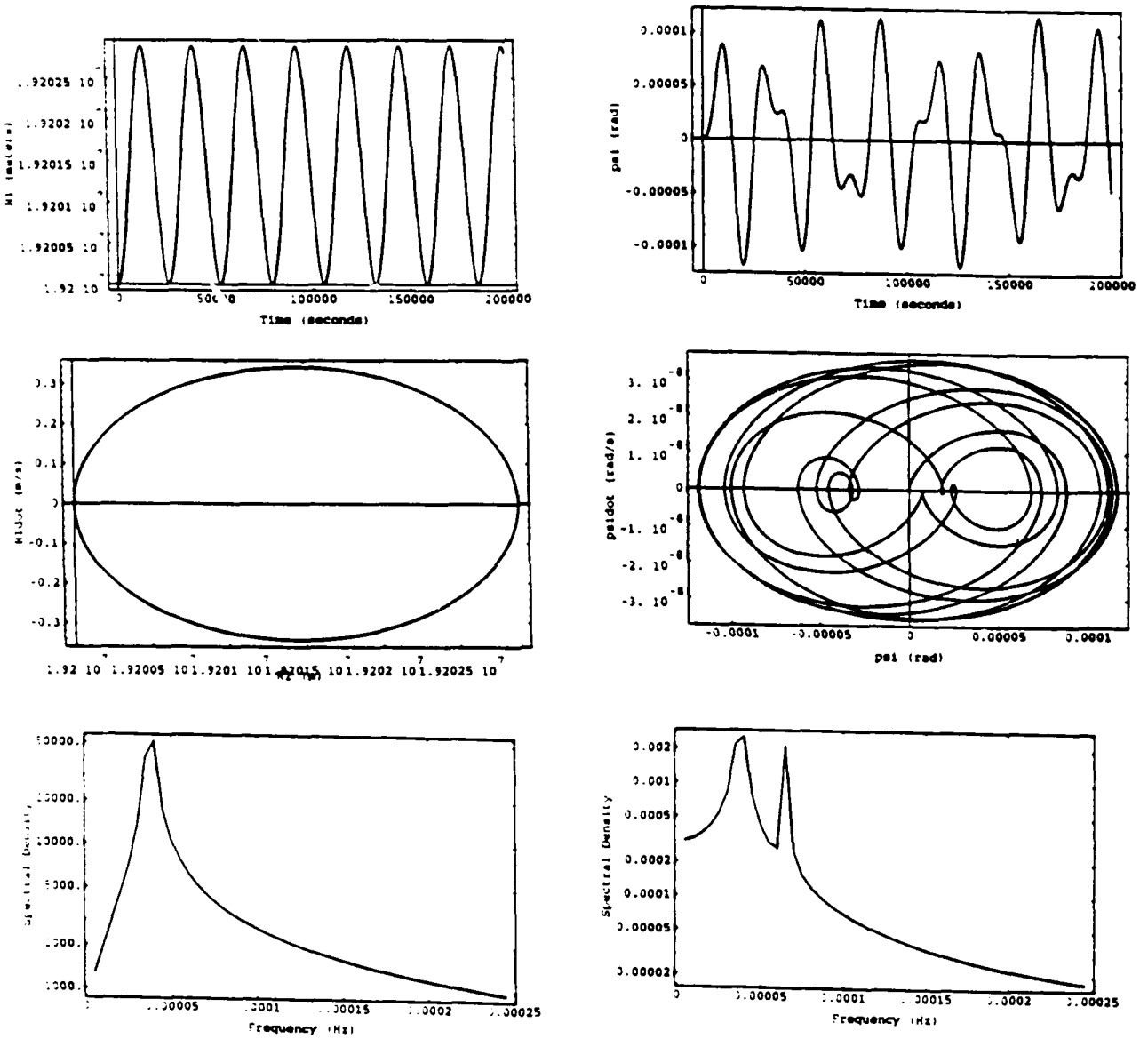

Figure 24: Orbital and Attitude Dynamics - Collapsed Dumbbell

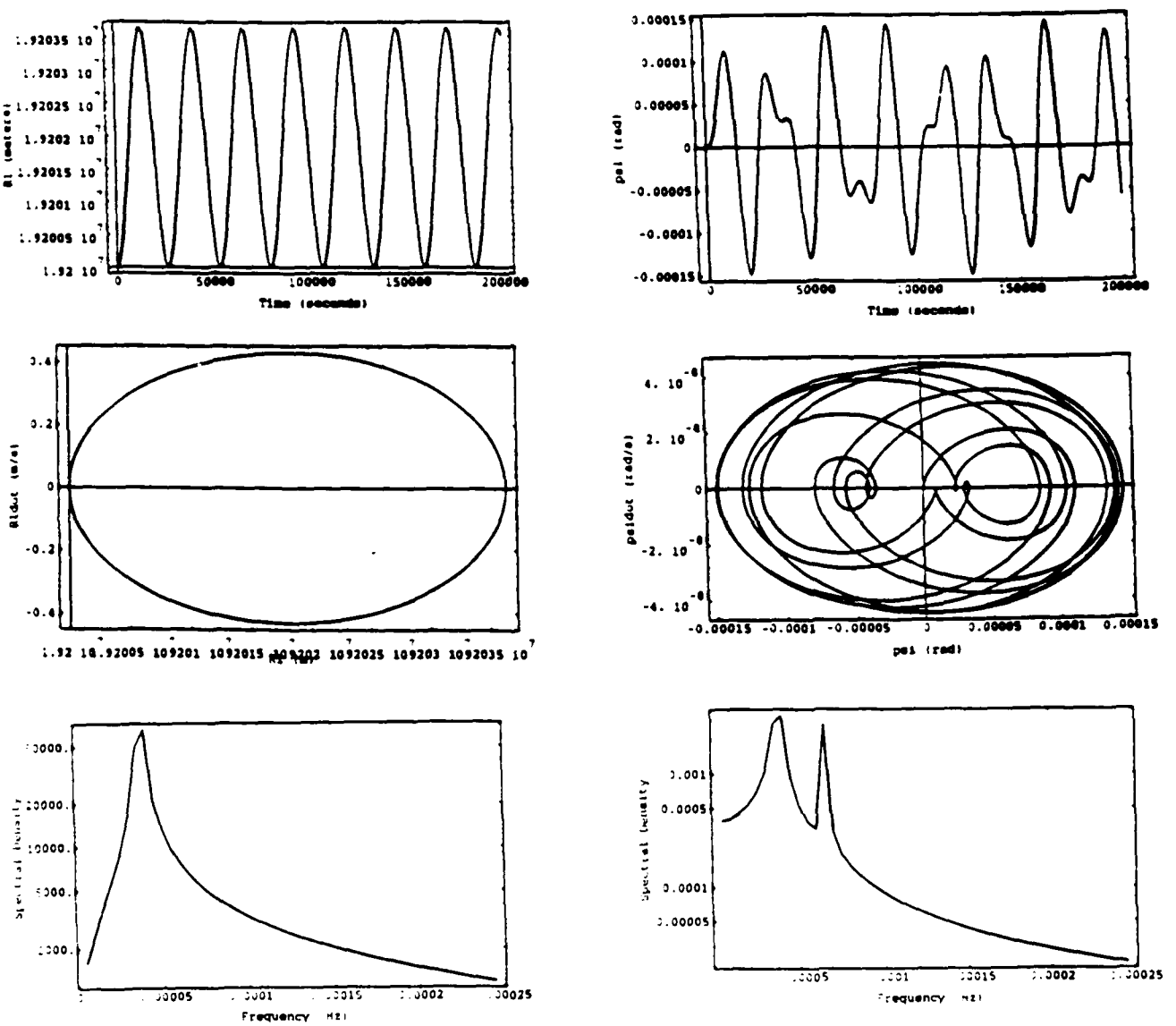

Figure 25: Orbital and Attitude Dynamics - 25% Deployed Dumbbell

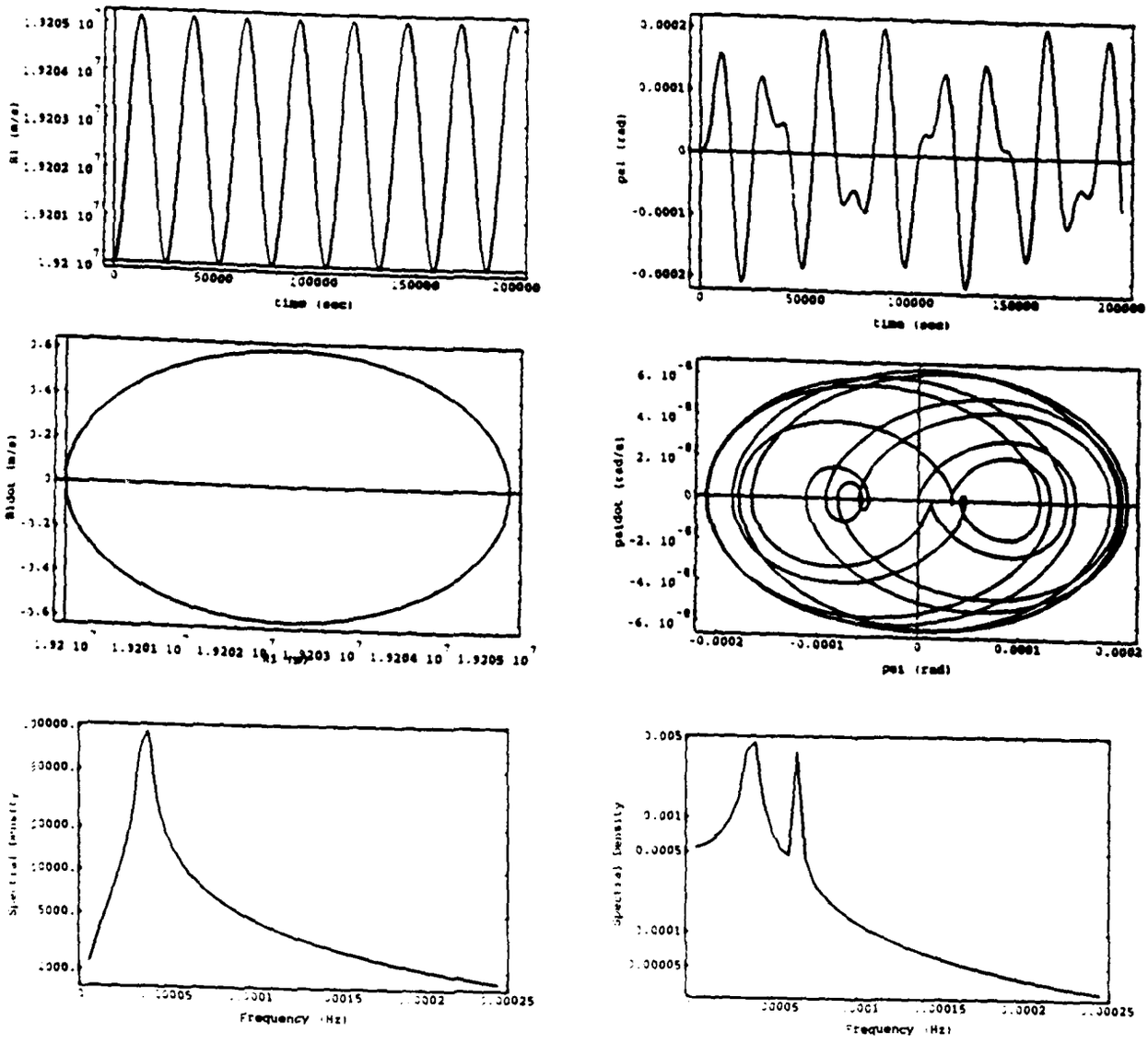

Figure 26: Orbital and Attitude Dynamics - 75% Deployed Dumbbell

and transitioning into a steady state elliptical orbit of 24.0 x 10^3 kilometer apogee and 19.2 x 10^3 kilometer perigee. The corresponding charts for the attitude motion show the same pattern of initial transient motion transitioning into a steady state of response. Several very interesting phenomena are evident in these charts. One is the very high frequencies associated with the transient phase of the attitude response, as indicated by the spectral density plot. The source of this has yet to be established. It can be observed further that the transient phase has at least three distinct regions with different amplitudes and rates of decay. These are most probably the result of jump phenomena. The high frequency transient behavior can also be observed in the phase-plane plot of the orbital motion where it is easily established that indeed several different regions of behavior do exist. An educated guess at this point is that the transition phase has regions of chaotic behavior between jumps.

The most interesting observation of the attitude motion is that the steady state configuration occurs at a negative ninety degree attitude orientation. The absence of any oscillations during this phase would signify that it is indeed an equilibrium state and the focus of a stable attractor. The initial vertical attitude configuration is thus unstable in the presence of deployment, and lies in the basin of attraction of the -90 degree attractor. To lend credence to these inferences, additional simulations were made for initial attitudes of ±10°, ±30°, and ±90°

The -90° run was to verify that it is the eye of a focus attractor. The results are shown in Figure 28 as orbital and attitude time histories and phase-plane plots. The orbital motion has no transient phase and is periodic indicating that a steady elliptical orbit is established from the start. The attitude motion does show a transient phase characterized by high frequency librations but settles to a steady state at the initial attitude with no attendant vibrations. These confirm this attitude as a stable equilibrium configuration. The -10° case resulted in the charts of Figure 29. They show the same behavior patterns as in the vertical orientation case, i.e. transient orbital and attitude motions with high frequency content, transitioning into a steady state equilibrium at -90° orientation. Thus both the zero and -10° attitudes lie in the basin of attraction of the -90° attractor.

A suspected attractor at +90° attitude was verified by simulation, the results of which are shown in Figure 30. The behavior is essentially the same as observed for the -90° case. At +10° attitude, the behavior pattern changed drastically compared to those observed so far. Figure 31 shows that the orbit is no longer elliptical. It is indeed hyperbolic, indicating that the satellite eventually escapes the earth's sphere of influence. The asymptotes occur at a true anomaly of about 7.8 radians indicating that the spacecraft executes one complete transition orbit around the earth before ending up on the hyperbolic flight path. The attitude motion plots show that the spacecraft "falls forward" very rapidly into alignment with the flight path (+90° attitude) while simultaneously executing very high frequency oscillations about this configuration. The oscillations start out quite large in amplitude but moderate somewhat during the transition orbit, and then builds up again once the hyperbolic orbit has been established. Thus for this initial configuration both the attitude and intended elliptical orbit are unstable. The +10° attitude lies in the basin of attraction of the +90° attractor. The orbit transitions from circular to hyperbolic.

These results indicate that initiating deployment from the 10° configuration results in instability of the orbit, landing the deploying spacecraft on an escape trajectory rather than an elliptical or circular orbit. Other attitude configurations in the vicinity of 10° can be expected to produce the same results. The range of such configurations was determined by additional simulations to be between 5° and 25°.

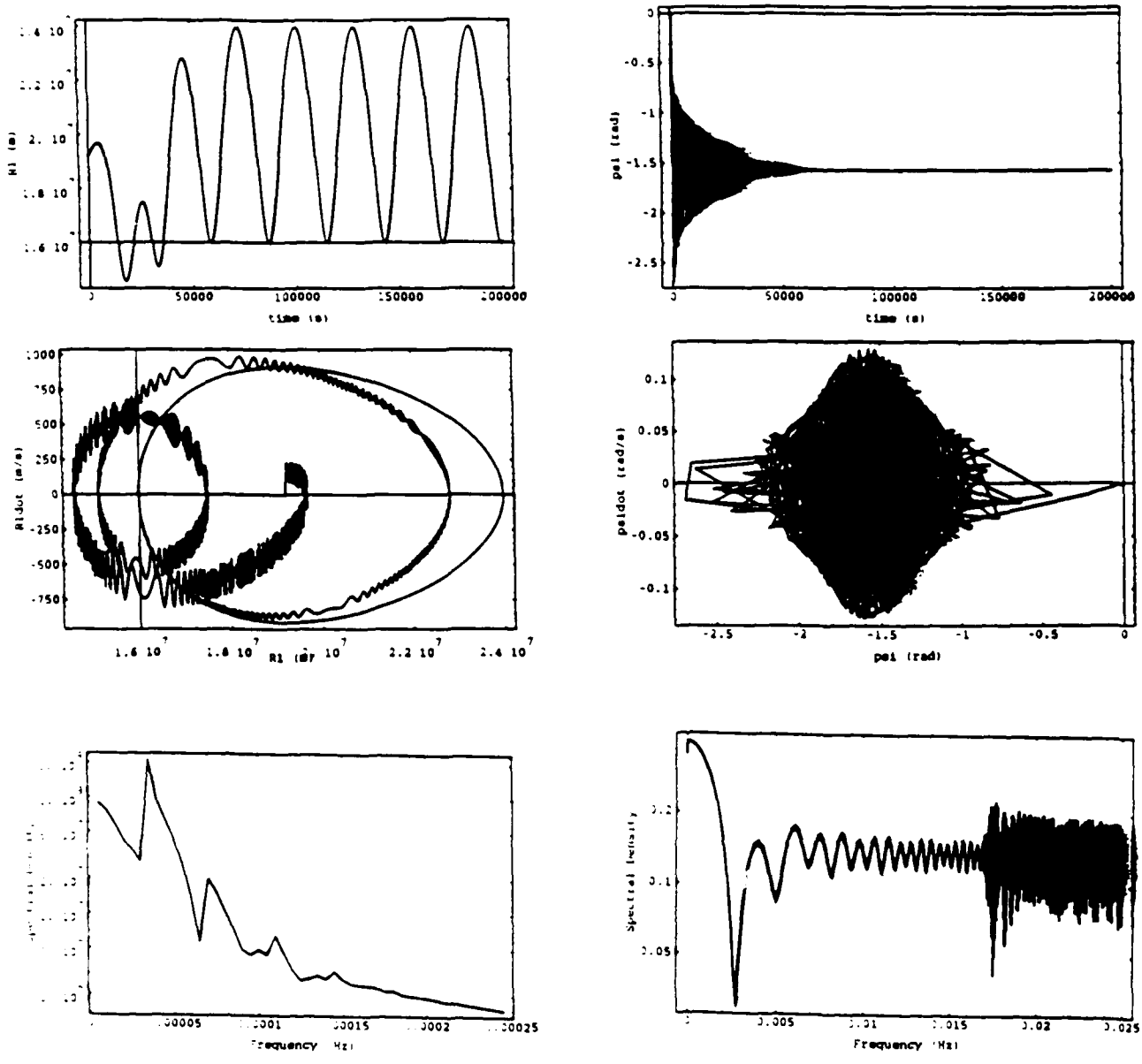

Figure 27: Satellite Deployment from Vertical Attitude

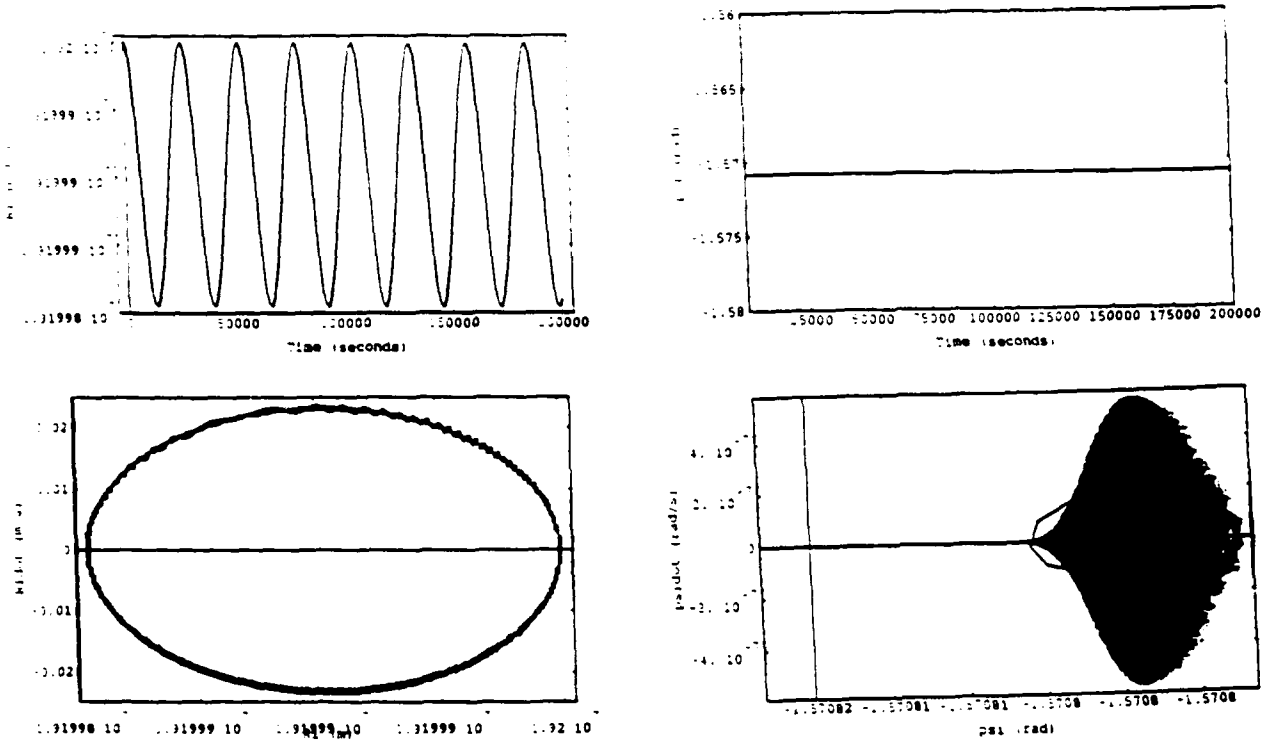

Figure 28: Satellite Deploying From Horizontal (-90°) Attitude

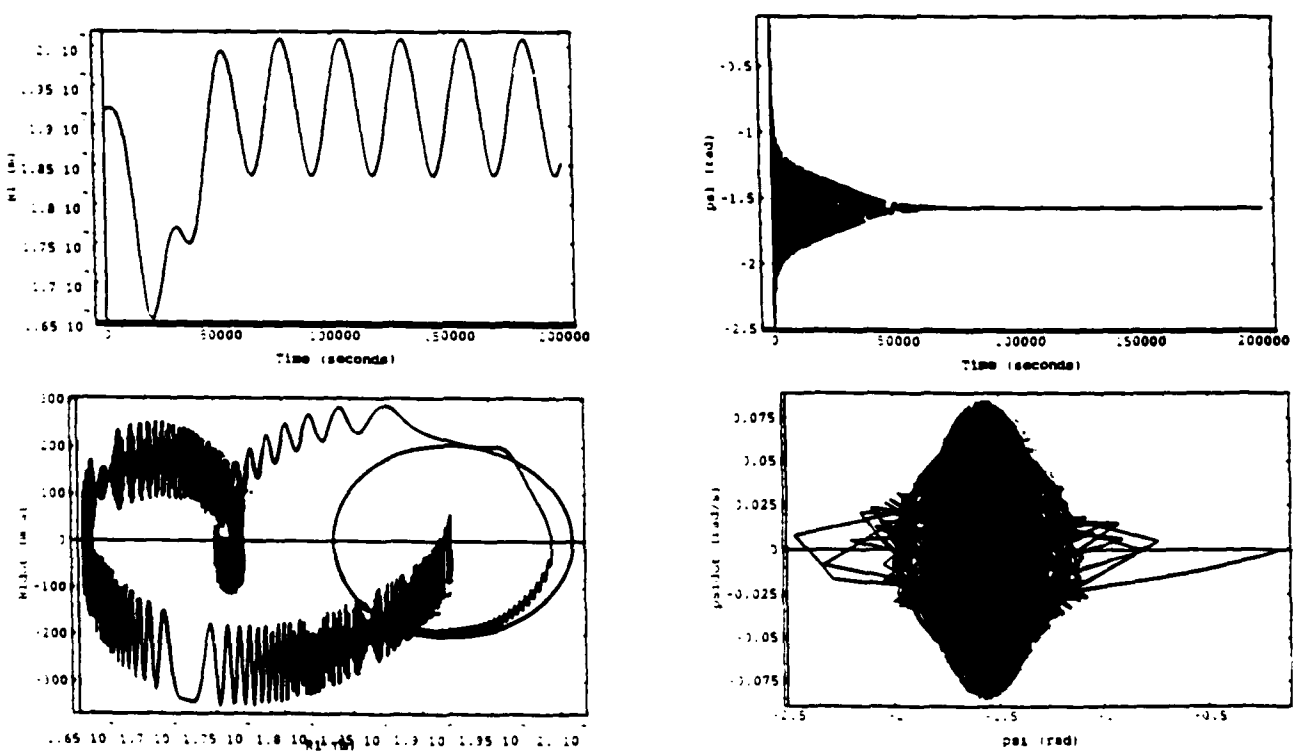

Figure 29: Satellite Deploying from -10° Attitude

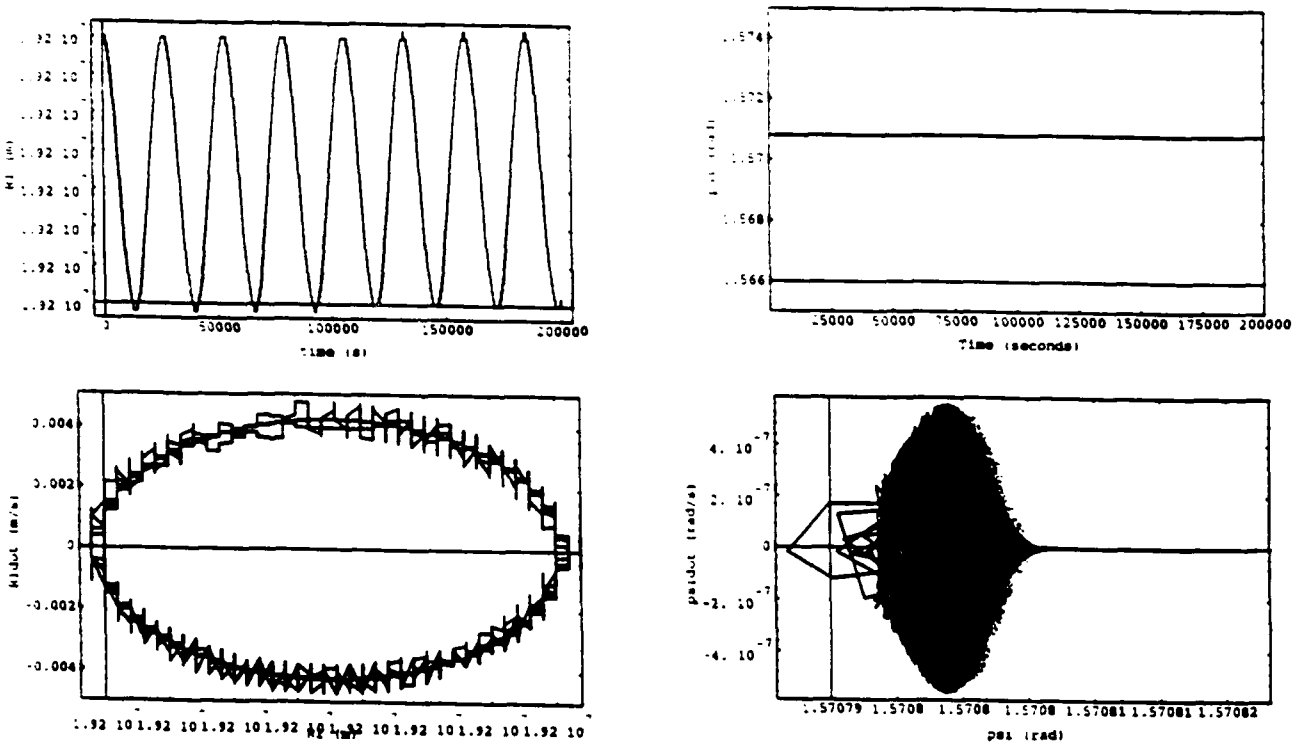

Figure 30: Satellite Deploying From +90° Attitude

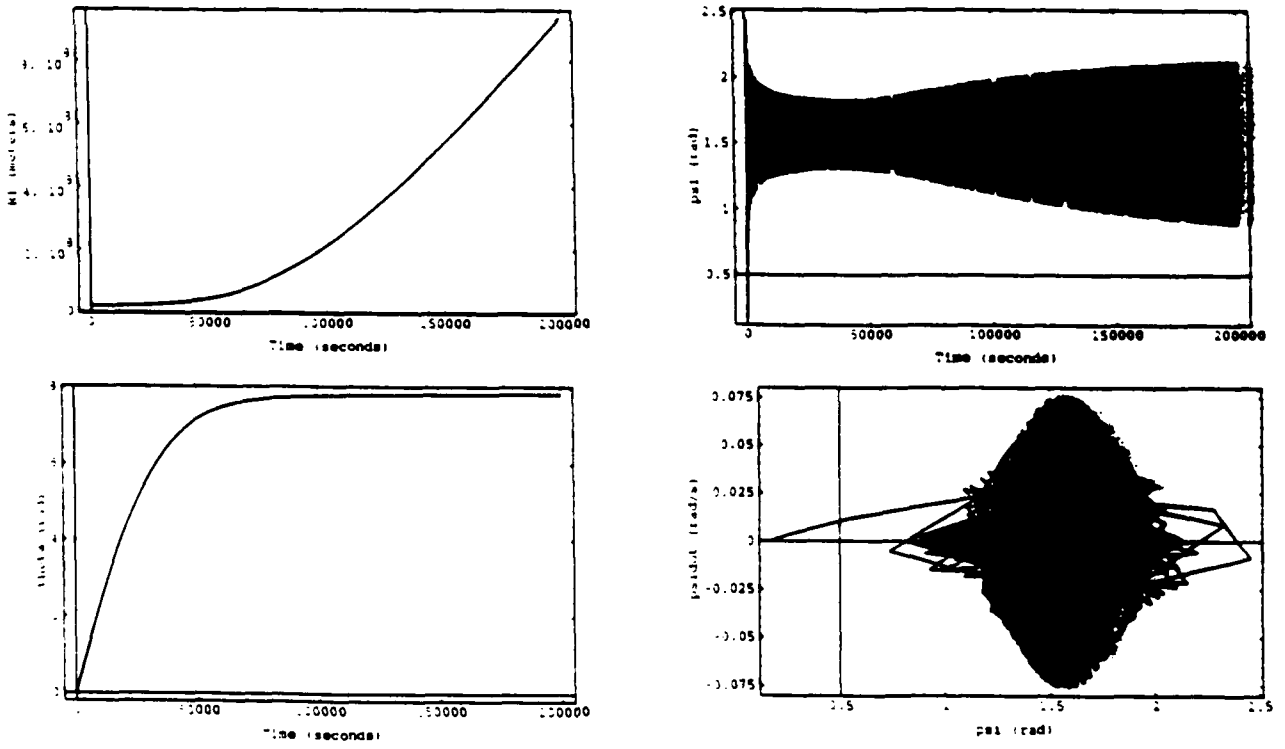

Figure 31: Satellite Deploying From +10° Attitude

(D) Summary

The accomplishments discussed above are here summarized and categorized as follows:

Dynamic Modeling:

We have developed a mathematical model for a flexible deployable dumbbell satellite that accounts for all the dynamic phenomena that would be encountered in applications: orbital dynamics, attitude dynamics, vibrational dynamics, and deployment dynamics. The resulting equations are highly coupled, highly nonlinear and very stiff. Because the state variables involved here consist of both discrete and continuous parameters (the orbital and attitude parameters are discrete, the vibrational and deployment ones are continuous), the equations are of the integro-differential form. The varying geometry due to deployment results in time varying boundary conditions. Thus solution of these boundary value problems are anything but standard.

We have partially validated the model by degenerating it to cases that have been studied by other investigators, and comparing ours with their models. The agreement in all cases has been perfect, giving us total confidence in our model.

Nonlinear Analytical Methodology:

In order to effectively address the nonstandard features of our model, we have developed techniques that represent rather unique and ingenious adaptations of standard numerical methods. An example is the use of finite difference discretization together with a summation approximation of integrals in order to reduce the integral portions of the equations to differential form. Another is the use of a perturbation analysis to avoid the difficulties inherent in stiff equation integration, and to simultaneously convert the nonlinear equations to piecewise semi-linear sets.

Dynamic Phenomenology:

We have used our model at different levels of degeneration to study important dynamic phenomena. We have established the vibration modal characteristics of a couple of deployment mechanisms in isolation from the orbital and attitude dynamics. In the process we have shown the existence of a modal agglomeration phenomenon associated with the telescopic deployment mechanism. We have studied the planar librational (attitude) dynamics of a rigid dumbbell as a function of the orbital eccentricity. With flexibility restored in this model, we have quantified the levels of librational and vibrational motions associated with standard maneuvers of orbit circularization and orbit transfers.

We have introduced the telescopic deployment mechanism into the planar rigid dumbbell and conducted extensive (but not exhaustive) simulation studies of orbital and attitude stability in the presence of deployment. We have shown that within the limitations of our constraint on the out-of-plane motions of the satellite, all attitude orientations other than the horizontal are unstable. For some of these orientations, the elliptical or circular orbit, necessary to maintain an orbit around a particular body, is also unstable: the satellite transitions to a hyperbolic (or parabolic)

orbit that eventually leads to the escape from the sphere of influence of the earth or other bodies around which orbit was intended.

FUTURE EFFORTS

Our research efforts will continue beyond the end of this funded project towards attainment of the broad goals of the project. Areas of research activity in the near future will include:

Complete validation of Current Model

The full capability of the current model encompasses the three dimensional motions of the classical dumbbell satellite, derived from the orbital, attitude, vibrational and deployment dynamics. Our validation to date has been based on restricting motions to the plane of the orbit and without consideration of deployment. This is because the bulk of previous investigations have been based on these same restrictions. Our simulations with the deployment feature were based on neglecting vibrational dynamics. While the results look reasonable and plausible, we have been unable to identify in the open literature similar studies to which we might compare our results. We believe these results are of a pioneering nature and hope that other investigators will be stimulated by our results to undertake similar studies and hence provide independent validation of our model. We will continue our efforts towards the goal of exercising our model in its full capability on simulations of practical situations.

Extensions to Current Model

The classical dumbbell satellite that we have considered so far assumes the two bodies to be point masses. To introduce more realism into the dumbbell as a generic spacecraft model, we plan to account for the rotary inertias of at least one of the bodies. This is a necessary step towards inclusion of attitude control into the simulations; an imperative feature if our model is to be applied to realistic systems. Eventually we hope to incorporate controls capabilities in all four constituent dynamics: orbital, attitude, vibration and deployment.

RESEARCH RELEVANCE

This research was initially motivated by the then high prospects for the development of large orbiting spacecraft systems in the near future. Recognizing that such systems would have to be configured in orbit by deployment and/or assembly of components, we identified the interaction of the configuration evolution dynamics with the other dynamic events associated with the orbit and attitude, as an area of needed basic research because of the lack of adequate understanding within the technical community of this interaction and its potential consequences.

The end of the cold war and the simultaneous downturn of global economies combined to eliminate almost completely the prospects for large space structures development. But this does not eliminate the need for the basic research identified here. One only has to consider the many problems plaguing our current space efforts that are attributable to in-orbit reconfigurations to realize the gravity of this need. The failure of the Galileo main antenna to deploy completely, the failure of the first shuttle mission to deploy a tethered subsatellite, and the loss of the Mars Observer satellite upon initiation of antenna deployment are spectacular examples of these problems. The need for this technology is as great as it ever was, large space structures or not.

Developing an appreciation for the consequences of configuration evolution on the in-flight performance and stability of spacecraft systems can be made only through analytical simulations with perhaps carefully planned and implemented space flight experimental validation. Laboratory experimental investigation is out of the question because the microgravity environment and the complex dynamic interactions can in no way be simulated experimentally at any cost.

This research is highly relevant to the identified need. It has demonstrated the effectiveness of rather simple models, *rich in the fundamental mechanic'* providing valuable insight into very complex phenomena. We are thankful to the Air Force Office of Scientific Research for its support of this study and we applaud the foresight and good judgement of the Program Manager, Dr. Spencer Wu, in investing in this critical technology development.

PUBLICATIONS

1. Amos, A.K., and Qu, B.,"The Dynamic Equations of Motion for a Deploying Telescopic Beam," *Proc. AIAA/ASME/ASCE/AHS 34th Structures, Structural Dynamics and Materials Conference*, April 1993.

2. Amos, A.K. "Variations in the Modal Characteristics of A Telescopically Deploying Beam," *Mechanics of Solids and Machines*, August 1993

3. Bell, E.J., and Amos, A.K., "Response of a Flexible Dumbbell Satellite to an Orbit Circularization Maneuver," *Proc. Ninth VPI&SU Symposium on Dynamics and Control of Large Structures*, May 10-12, 1993.

4. Cohrac, J.R., and Amos, A.K., "Orbital Eccentricity Effects in Satellite Librations," *Proc. Eighth VPI&SU Symposium on Dynamics and Control of Large Structures*, May 6-8, 1991.

5. Amos, A.K., Melton, R.C., and Thompson, R.G. "Orbital Equations of a Flexible Dumbbell Satellite - Part 1", *Proc. AIAA/AAS Astrodynamics Conference*, Portland, OR, August 20-22, 1990.

6. Qu, B. and Amos, A.K., "Orbital and Attitude Stability of a Telescopically Deploying Dumbbell Satellite," under preparation.